

Y U M S 97-7
 S N U T P 97-035
 M arch 25, 2024

CP Violation in the Top-Quark Pair Production at a Next Linear Collider

M .S.Baek, S.Y .Choi and C .S.K im

Department of Physics, Yonsei University, Seoul 120-749, Korea

Abstract

We provide a detailed, model-independent, study for CP violation effects due to the T-odd top-quark electric dipole moment (EDM) and weak dipole moment (WDM) in the top-quark pair production via e^+e^- and two-photon annihilation at a next e^+e^- linear collider (NLC). There are two methods in detecting CP violation effects in these processes. One method makes use of measurements of various spin correlations in the final decay products of the produced top-quark pair, while the other is to measure various CP-odd polarization asymmetry effects of the initial states. In the e^+e^- case only the first method can be used, and in the $\gamma\gamma$ case both methods can be employed. We provide a complete classification of angular correlations of the t and \bar{t} decay products under CP and CP T which greatly facilitate CP tests in the e^+e^- mode. Concentrating on the second method with the Compton back-scattered high-energetic laser light off the electron or positron beam in the two-photon mode, we construct two CP-odd and CP T-even initial polarization configurations and apply them to investigating CP-violating effects due to the top-quark EDM. With a typical set of experimental parameters at the NLC, we compare the 1- sensitivities to the top-quark EDM and WDM in the e^+e^- mode and the two-photon mode. Some model expectation values of the T-odd parameters are compared with the results.

1 Introduction

Precision measurements of various production and decay modes of the top quark are expected to provide useful information on physics beyond the SM. Testing new physics in observables which are sensitive to CP violation seems especially promising. As the top quark hardly mixes with other generations, the GIM mechanism of unitarity constraints leads to negligibly small effects of CP violation in the SM. Thus, observation of CP non-invariance in top-quark physics would definitely be a signal for physics beyond the SM.

An important property of heavy top ($m_t = 175 \text{ GeV}$) [1] is that hadronization of the top quark can be neglected to a good approximation because on average it decays before it can form hadronic bound states [2]. This implies in particular that spin effects, for instance spin correlations between the produced t and \bar{t} quarks are not severely distorted by hadronization. These spin effects can be analyzed through the distributions and angular correlations of the weak decay products of the t and \bar{t} quarks. Moreover, these effects can be calculated in perturbation theory. Hence they provide an additional means of testing the SM predictions and of searching for possible new physics effects in top quark production and decay.

The $t\bar{t}$ coupling consists of the SM tree-level and the magnetic dipole moment (MDM) couplings as well as the EDM coupling. Likewise, in addition to the tree-level SM $Z t\bar{t}$ coupling, we have the analogous Z MDM and Z EDM couplings, the latter of which is called the top-quark WDM. In both cases these couplings may have imaginary parts. The MDM-like couplings are present in the SM at the one-loop level. On the other hand, the EDM-like couplings violate CP and, due to the structure of the SM, they are only present perturbatively in the SM at the three loop level. In some extensions to the SM, however, EDM couplings may be present at lower order in perturbation theory. Some models [3] which can give relatively large fermion EDM's include left-right symmetric theories, additional Higgs multiplets, supersymmetry, and composite models. Neglecting the MDM-like couplings, we consider both the T-odd top-quark EDM and WDM in the reactions $e^+e^- \rightarrow t\bar{t}$ and $\gamma \rightarrow t\bar{t}$ at NLC [4].

Previously CP violation in the process $e^+e^- \rightarrow t\bar{t}$ has been extensively investigated. Those previous works can be classified in two categories according to their own emphasized aspects: (i) the classification [5, 6, 7, 8] of spin correlations of the t and \bar{t} decay products without electron beam polarization, and (ii) the use of a few typical CP-odd observables with electron beam polarization [9, 10]. In the first class they have constructed all the CP-odd observables according to their ranks. However, since the t and \bar{t} are spin-1/2 particles, the CP-odd spin correlation only up to rank-two can appear in the process. Therefore, all the constructed CP-odd observables previously investigated are not linearly independent. In the present work we completely define all the linearly-independent CP-odd correlations by which all other CP-odd correlations can be expressed. In the second class, it has been shown that electron beam polarization is very crucial for a few specialized CP-odd correlations. We extend their works to investigate which CP-odd correlations depend crucially on electron polarization and which ones do not. After expressing all the strongly-dependent CP-odd correlations in terms of the linearly-independent correlations we can provide simple explanations for why those specialized observables depend crucially on electron beam polarization.

Detailed studies have been performed mainly in the processes $e^+e^- \rightarrow t\bar{t}$ including general studies of $t\bar{t}$, $t\bar{t}Z$ and $t\bar{t}W$ couplings [5, 6, 7, 8] previously. A photon linear collider (PLC),

employing polarized photons by the Compton back-scattering of polarized laser light on electron/positron beams of NLC, enables us to measure the tt and $t\bar{t}W$ couplings and to investigate the possibility of extracting the effective couplings of the top quark to the photon.

We can employ two methods to extract the top-quark effective couplings at a PLC. One method makes use of the quasi-freely decaying property [2] of the top quark by measuring various spin correlations in the tt final system, $(b\bar{W}^+)(b\bar{W}^-)$ or $(bf_1f_2)(bf_3f_4)$. The other method is to employ linearly-polarized photon beams to measure various polarization asymmetries of the initial states. It is, of course, possible to combine the two methods. The former technique is essentially same as that employed in e^+e^- collisions [6, 7, 8] with one difference; in e^+e^- collisions the spin of the tt system is restricted to $J = 1$, while in photon fusion $J = 0$ or $J = 2$ is allowed.

Section 2 is devoted to the introduction of the top-quark EDM and WDM, and to some model expectations for the CP-odd parameters. In Section 3 we classify all angular dependences and angular correlations of t and \bar{t} decay products in the e^+e^- mode under CP and CPT transformations, where T is the "naive" time reversal operation which flips particle momenta and spins but does not interchange initial and final states. Then we apply the CP-odd angular correlations to probing CP violation due to the top-quark EDM and WDM in the e^+e^- mode by considering the polarized electron case as well as the unpolarized electron case.

In Section 4 we give a detailed description of the energy spectrum and polarization of the high-energy Compton backscattered light. The study of CP violation in the two-photon mode [11] is extended in Section 5, where we construct two CP-odd and CPT-even initial photon polarization configurations, and apply them to obtain the 1- sensitivities of the top-quark EDM without the detailed information on the complicated t and \bar{t} decay patterns.

After comparing the 1- sensitivities to the top-quark EDM in the e^+e^- mode and the two-photon mode, we close Section 6 with some prospects for further studies related with CP violation.

The Appendices are devoted to the definition and explicit form of the angular distributions P_x and the definition of the angular correlations D and D^0 .

2 Top-quark EDM

One of the most commonly studied CP-violating operators is the EDM of a fermion and its generalizations to weak and strong couplings. The most general matrix element of the electromagnetic current between two top-quark spinors contain T-odd term:

$$i\bar{u}(p_2)\gamma^\mu u(p_1) = iF_3(q^2)\bar{u}(p_2)\gamma^\mu\gamma^5 u(p_1); \quad (1)$$

The value of this form factor at zero-momentum transfer:

$$F_3(q^2 = 0) = d_t; \quad (2)$$

is called the EDM. This induces a local interaction that can be derived from the effective Lagrangian:

$$\mathcal{L}_{\text{eff}}^d = \frac{1}{2}d_t\bar{u}i\gamma^5 u F + \frac{1}{2}d_t^Z\bar{u}i\gamma^5 u Z + \frac{1}{2}d_t^g\bar{u}i\gamma^5 u G_a; \quad (3)$$

where we have also added the generalizations to fermion couplings to the Z boson and gluons.

The quark EDM in the SM vanishes at the one-loop order, because of the unitarity of CKM matrix. Diagrams at two-loop order can have a CP-violating phase, but it has been shown by Shabalin [12] that the sum of two-loop contributions to $F_3(q^2 = 0)$ vanishes. It is thus thought that the lowest-order SM contribution to the quark EDM occurs at least at the three-loop level.

There are models which generate a non-zero quark EDM at the one-loop level. Typical examples are the models of CP violation with extra scalars [13]. When CP violation comes from the exchange of a neutral Higgs boson, the EDM for up-type quarks, down-type quarks, or charged leptons is given in the $M_H \rightarrow m_f$ limit by:

$$d_f = \frac{e Q_f}{32} \frac{2 G_F}{M_H^2} m_f^3 \frac{\text{Re}(A) \text{Im}(A)}{M_H^2} \log \frac{m_H^2}{M_f^2}; \quad (4)$$

where A is a dimensionless parameter for the Higgs coupling with the left-handed fermion. This is largest for the top-quark although in the case of the top-quark it may be a poor approximation to take $q^2 = 0$. In the case where the CP violation arises in the charged scalar sector, the EDM for down-type quarks is given by

$$d_d = e \frac{2 G_F}{12} m_d \text{Im}(\kappa_1) \mathcal{V}_{td} \frac{x_t}{(1-x_t)^2} \left[\frac{3}{4} - \frac{5}{4} x_t + \frac{1}{1-x_t} \log x_t \right]; \quad (5)$$

where κ_1 and κ_2 are dimensionless parameters for the charged Higgs coupling with fermions, and $x_t = m_t^2/M_H^2$. This result follows from the dominance of the top-quark in the loop and assumes that the dominant contribution comes from the lightest charged scalar H^\pm . For the case of an up-type quark the result is:

$$d_u = e \frac{2 G_F}{12} m_u \text{Im}(\kappa_1) \frac{x_t}{(1-x_t)^2} \sum_i \mathcal{V}_{ui}^2 x_i \left[\frac{1}{2} - \frac{3x_i}{(1-x_i)} \log x_i \right]; \quad (6)$$

We denote the $t\bar{t}$ and $Z t\bar{t}$ couplings by the vertex factor $i e \Gamma^V$ (See Figure 1), where

$$\Gamma^V = \gamma_\mu + a_V \gamma_5 + \frac{c_V}{2m_t} \not{q} \gamma_5; \quad V = \gamma; Z; \quad (7)$$

with the vector and axial-vector couplings of the t quark given in the SM by

$$v = \frac{2}{3}; \quad a = 0; \quad v_z = \frac{(\frac{1}{4} - \frac{2}{3} x_w)}{x_w (1-x_w)}; \quad a_z = \frac{1}{4 x_w (1-x_w)}; \quad (8)$$

and $x_w = \sin^2 \theta_w$, θ_w being the weak mixing angle. Here, q is the four-momentum of the vector boson, $V (= \gamma; Z)$. For $x_w = 0.23$, we find that $v_z = 0.23$ and $a_z = 0.59$. We assume that the only additional couplings to the SM ones are the CP-violating EDM and WDM factors,

$$d_t^{\gamma Z} = \frac{e}{m_t} c_{\gamma Z} \quad 1.13 \times 10^{16} c_{\gamma Z} \text{ (cm)}; \quad (9)$$

for $m_t = 175 \text{ GeV}$, and that the CP-violating form factors, $c_{\gamma Z}$ are small.

3 Electron-positron mode

3.1 Helicity amplitudes for top-quark pair production

We define the helicities of the t and \bar{t} in the e^+e^- c.m. frame. Let us define the coordinate system F_0 for the $t\bar{t}$ production process, $e^+e^- \rightarrow t\bar{t}$. The scattering is in the x - z plane and the z -axis is along the top-quark momentum direction. The y -axis is along $\mathbf{p}_e \times \mathbf{p}_{\bar{e}}$ and the x -axis is given by the right-handed rule.

We calculate the polarization amplitudes $M_{\lambda_1\lambda_2\lambda_3\lambda_4} = e^2 M_{\lambda_1\lambda_2\lambda_3\lambda_4}$ for the production process $e^+e^- \rightarrow t\bar{t}$ by using a very straightforward and general method [14] based on two-component spinors. The helicity amplitudes $M_{\lambda_1\lambda_2\lambda_3\lambda_4}$ are presented in the e^+e^- c.m. frame where the positive z -axis is chosen along the top quark momentum direction :

$$\begin{aligned} \mathbf{p}_e &= \frac{p_{\bar{s}}}{2} (1; \sin\theta; 0; \cos\theta); & \mathbf{p}_{\bar{e}} &= \frac{p_{\bar{s}}}{2} (1; \sin\theta; 0; -\cos\theta); \\ \mathbf{p}_t &= \frac{p_{\bar{s}}}{2} (1; 0; 0; 1); & \mathbf{p}_{\bar{t}} &= \frac{p_{\bar{s}}}{2} (1; 0; 0; -1); \end{aligned} \quad (10)$$

Then the helicity amplitudes of the process $e^+e^- \rightarrow t\bar{t}$ can be expressed in a compact fashion as follows

$$\begin{aligned} M_{\lambda_1\lambda_2\lambda_3\lambda_4} &= \frac{1}{s} \sum_{\lambda=L,R} \sum_{\lambda_0=0,\pm} X_{\lambda\lambda_0}^{\lambda_1\lambda_2} (v + a_0) J^e(\lambda_3; \lambda_4) J^t(\lambda_1; \lambda_2) \\ &\quad + \frac{i}{2m_t s} \sum_{\lambda=L,R} X_{\lambda\lambda_0}^{\lambda_1\lambda_2} c^h S^e(\lambda_3; \lambda_4) P^t(\lambda_1; \lambda_2); \end{aligned} \quad (11)$$

where

$$\begin{aligned} J^e(\lambda_3; \lambda_4) &= v(\mathbf{p}_e; \lambda_3) P u(\mathbf{p}_e; \lambda_4); & J^t_0(\lambda_1; \lambda_2) &= u(\mathbf{p}_t; \lambda_1) P v(\mathbf{p}_t; \lambda_2); \\ S^e(\lambda_3; \lambda_4) &= 2v(\mathbf{p}_e; \lambda_3) \not{\mathbf{p}}_t P u(\mathbf{p}_e; \lambda_4); & P^t(\lambda_1; \lambda_2) &= u(\mathbf{p}_t; \lambda_1) \not{\mathbf{p}}_e v(\mathbf{p}_t; \lambda_2); \end{aligned} \quad (12)$$

with $\lambda = L, R$, $\lambda_0 = 0, \pm$, and $P_{R,L} = P = \frac{1}{2}(1 \pm \gamma_5)$.

In the vanishing electron mass limit, the positron helicity should be opposite to the electron helicity [15], that is to say, $M_{LL; \lambda_3\lambda_4} = M_{RR; \lambda_3\lambda_4} = 0$. Therefore, it is convenient to rewrite $M_{LR; \lambda_3\lambda_4} = M^L$ and $M_{RL; \lambda_3\lambda_4} = M^R$, which are given by

$$M^L = (v_L - a_L)(1 - \cos\theta); \quad M^L = \frac{p_{\bar{s}}}{2m_t} 4 \frac{m_t^2}{s} v_L i c_L \sin\theta; \quad (13)$$

for the initial $e_L e_R^+$ configuration, and

$$M^R = (v_R - a_R)(1 - \cos\theta); \quad M^R = \frac{p_{\bar{s}}}{2m_t} 4 \frac{m_t^2}{s} v_R i c_R \sin\theta; \quad (14)$$

for the initial $e_R e_L^+$ configuration with the scattering angle θ and the dimensionless variables defined as

$$\begin{aligned} v_L &= v + r_L v_z; & v_R &= v + r_R v_z; \\ a_L &= a + r_L a_z; & a_R &= a + r_R a_z; \\ c_L &= c + r_L c_z; & c_R &= c + r_R c_z; \end{aligned} \quad (15)$$

Here the two \sqrt{s} -dependent parameters r_L and r_R in the SM are defined as

$$\begin{aligned} r_L &= \frac{\frac{1}{2} \frac{x_W}{1 - \frac{m_Z^2}{s}}}{\frac{x_W}{1 - \frac{m_Z^2}{s}} (1 - x_W)} + 0.64 \frac{1}{s} \frac{m_Z^2}{s}^{1/2}; \\ r_R &= \frac{\frac{x_W}{1 - \frac{m_Z^2}{s}}}{\frac{x_W}{1 - \frac{m_Z^2}{s}} (1 - x_W)} - 0.55 \frac{1}{s} \frac{m_Z^2}{s}^{1/2}; \end{aligned} \quad (16)$$

where we have inserted $x_W = 0.23$ and have neglected the Z boson width Γ_Z , which is easily incorporated but its numerical effect is minute for $\sqrt{s} = 2m_t$ since $\frac{\Gamma_Z}{s} = \frac{1}{7} \cdot 10^{-3}$.

3.2 Top and anti-top quark decays

We calculate the helicity amplitudes of $t \rightarrow W^+ b$ and $t \rightarrow W^- b$ for on-shell W bosons. For the process $t \rightarrow W^+ b$, the top quark is taken to decay in its rest frame where the top quark momentum is $p_t = (m_t; 0; 0; 0)$. Spherical coordinates are used to describe the outgoing particles; the polar angle θ is taken from the positive z axis and the azimuthal angle ϕ is taken from the positive x axis in the x-y plane. The bottom quark and W boson are taken on their mass shells with the four-momenta p_b (p_W) for the bottom (anti-)quark and the four-momenta p_W (p_b) for the W^+ (W^-) bosons taken as

$$\begin{aligned} p_b &= E_b (1; \sin \theta \cos \phi; \sin \theta \sin \phi; \cos \theta); \\ p_W &= E_W (1; \sin \theta \cos \phi; \sin \theta \sin \phi; \cos \theta); \\ p_b &= E_b (1; \sin \theta \cos \phi; \sin \theta \sin \phi; \cos \theta); \\ p_W &= E_W (1; \sin \theta \cos \phi; \sin \theta \sin \phi; \cos \theta); \end{aligned} \quad (17)$$

where we neglect the bottom quark mass, which is about 5 GeV, and then

$$E_b = \frac{m_t^2 - m_W^2}{2m_t}; \quad E_W = \frac{m_t^2 + m_W^2}{2m_t}; \quad \sin \theta = \frac{E_b}{E_W}. \quad (18)$$

The angles θ and ϕ in the t (\bar{t}) decay refer to the direction of the W^+ (W^-) boson. We denote the helicity amplitudes as $M_{h_t; h_W h_b}^W$ and as $M_{h_t; h_W h_b}^W$ after extracting a common factor as

$$\begin{aligned} M_{h_t; h_W h_b}^W &= \frac{e}{2 \sin \theta_W} \sqrt{\frac{m_t^2 - m_W^2}{m_t^2 + m_W^2}} h_{h_t; h_W h_b}^W; \\ M_{h_t; h_W h_b}^W &= \frac{e}{2 \sin \theta_W} \sqrt{\frac{m_t^2 - m_W^2}{m_t^2 + m_W^2}} h_{h_t; h_W h_b}^W. \end{aligned} \quad (19)$$

There are four non-vanishing helicity amplitudes for each decay mode in the rest frame of the top quark and the top anti-quark for $m_b = m_{\bar{b}} = 0$:

$$h_{\frac{1}{2}; \frac{1}{2} \frac{1}{2}} = \frac{m_t}{m_W} \sin \frac{\theta}{2}; \quad h_{\frac{1}{2}; \frac{1}{2} \frac{-1}{2}} = \frac{m_t}{m_W} \cos \frac{\theta}{2};$$

$$h^+; 0 \rightarrow i_t = \frac{m_t}{m_W} \cos \frac{\theta}{2} e^{i\phi}; \quad h^+; \frac{1}{2} \rightarrow i_t = \frac{P}{2} \sin \frac{\theta}{2} e^{i\phi}; \quad (20)$$

$$h^+; 0 \rightarrow i_t = \frac{m_t}{m_W} \cos \frac{\theta}{2} e^{-i\phi}; \quad h^+; + \rightarrow i_t = \frac{P}{2} \sin \frac{\theta}{2} e^{-i\phi};$$

$$h^-; 0 \rightarrow i_t = \frac{m_t}{m_W} \sin \frac{\theta}{2}; \quad h^-; + \rightarrow i_t = \frac{P}{2} \cos \frac{\theta}{2}; \quad (21)$$

The helicity amplitudes can be used to derive the density matrix of the top quark. When the W polarization is not measured, the t and \bar{t} decay density matrices are given by

$$D_t = \frac{1}{2} \begin{pmatrix} 1 + \frac{m_t^2}{m_W^2} \cos \theta & \frac{m_t}{m_W} \sin \theta e^{i\phi} \\ \frac{m_t}{m_W} \sin \theta e^{-i\phi} & 1 - \frac{m_t^2}{m_W^2} \cos \theta \end{pmatrix};$$

$$D_{\bar{t}} = \frac{1}{2} \begin{pmatrix} 1 + \frac{m_t^2}{m_W^2} \cos \theta & \frac{m_t}{m_W} \sin \theta e^{i\phi} \\ \frac{m_t}{m_W} \sin \theta e^{-i\phi} & 1 - \frac{m_t^2}{m_W^2} \cos \theta \end{pmatrix}; \quad (22)$$

respectively, where the polarization efficiency ϵ_W is given by

$$\epsilon_W = \frac{m_t^2 - 2m_W^2}{m_t^2 + 2m_W^2} = 0.41; \quad (23)$$

for $m_t = 175 \text{ GeV}$ and $m_W = 80 \text{ GeV}$.

We now discuss the angular distributions of the leptons arising from semileptonic decays

$$t \rightarrow W^+ (p_W) b \rightarrow l^+ (p_l) \bar{\nu}_b (p_{\bar{\nu}});$$

$$\bar{t} \rightarrow W^- (p_W) \bar{b} \rightarrow l^- (p_l) \nu_b (p_{\nu}); \quad (24)$$

for the polarized t and \bar{t} quarks, where the momenta in the parentheses refer to the rest systems of t and \bar{t} and serve to analyze the spin polarization of t and \bar{t} . Neglecting lepton masses we write the lepton momenta as

$$p_l = E_l (1; \sin \theta_l \cos \phi_l; \sin \theta_l \sin \phi_l; \cos \theta_l);$$

$$p_{\bar{\nu}} = E_{\bar{\nu}} (1; \sin \theta_{\bar{\nu}} \cos \phi_{\bar{\nu}}; \sin \theta_{\bar{\nu}} \sin \phi_{\bar{\nu}}; \cos \theta_{\bar{\nu}});$$

$$p_l = E_l (1; \sin \theta_l \cos \phi_l; \sin \theta_l \sin \phi_l; \cos \theta_l);$$

$$p_{\nu} = E_{\nu} (1; \sin \theta_{\nu} \cos \phi_{\nu}; \sin \theta_{\nu} \sin \phi_{\nu}; \cos \theta_{\nu}); \quad (25)$$

where E_{l^+} and E_{l^-} are the lepton energies and $E_{\bar{\nu}_b}$ and E_{ν_b} the neutrino energies in the t and \bar{t} rest frames, respectively. We denote the helicity amplitudes as $M_{h_t}^1$ and as $M_{h_t}^2$ after extracting a common factor as follows

$$M_{h_t}^1 = 2g^2 \frac{q \sqrt{(m_t^2 - q^2) E_{l^+} E_{\bar{\nu}_b}}}{q^2 m_W^2 + i m_W \Gamma_W} h_{h_t} h_{\bar{\nu}_b}^1;$$

$$M_{h_t}^2 = 2g^2 \frac{q \sqrt{(m_t^2 - q^2) E_{l^-} E_{\nu_b}}}{q^2 m_W^2 + i m_W \Gamma_W} h_{h_t} h_{\nu_b}^1; \quad (26)$$

In the semileptonic decays, there are two non-vanishing helicity amplitudes for each decay mode in the rest frames of the top quark and the top anti-quark for $m_b = m_{\bar{b}} = 0$:

$$\begin{aligned}
h_+; \bar{l} &= \cos \frac{\theta_1}{2} \cos \frac{\theta_b}{2} \sin \frac{\phi_1}{2} e^{i\phi_1} & \sin \frac{\theta_b}{2} \cos \frac{\phi_1}{2} e^{i\phi_b}; \\
h_-; \bar{l} &= \sin \frac{\theta_1}{2} e^{i\phi_1} \cos \frac{\theta_b}{2} \sin \frac{\phi_1}{2} e^{i\phi_1} & \sin \frac{\theta_b}{2} \cos \frac{\phi_1}{2} e^{i\phi_b}; \\
h_+; l &= \cos \frac{\theta_1}{2} \cos \frac{\theta_b}{2} \sin \frac{\phi_1}{2} e^{-i\phi_1} & \sin \frac{\theta_b}{2} \cos \frac{\phi_1}{2} e^{-i\phi_b}; \\
h_-; l &= \sin \frac{\theta_1}{2} e^{-i\phi_1} \cos \frac{\theta_b}{2} \sin \frac{\phi_1}{2} e^{-i\phi_1} & \sin \frac{\theta_b}{2} \cos \frac{\phi_1}{2} e^{-i\phi_b};
\end{aligned} \tag{27}$$

It is well known that within the SM the angular distribution of the charged lepton is a much better spin analyzer of the top quark than that of the b quark or the W -boson arising from semi- or non-leptonic t decays. As a matter of fact, the decay matrices of the semileptonic decays of polarized t and \bar{t} are given in the t and \bar{t} helicity bases by

$$D_t^{\frac{1}{2}} = \frac{1}{2} \begin{pmatrix} 1 + \cos \theta_1 & \sin \theta_1 e^{i\phi_1} \\ \sin \theta_1 e^{-i\phi_1} & 1 - \cos \theta_1 \end{pmatrix}; \tag{28}$$

$$D_{\bar{t}}^{\frac{1}{2}} = \frac{1}{2} \begin{pmatrix} 1 + \cos \theta_1 & \sin \theta_1 e^{i\phi_1} \\ \sin \theta_1 e^{-i\phi_1} & 1 - \cos \theta_1 \end{pmatrix}; \tag{29}$$

respectively. θ_1 and ϕ_1 are the polar and azimuthal angles of l^+ from the t decay, which are defined in the t rest frame F_t constructed by boosting the tt c.m. frame F_0 along the top quark momentum direction. Similarly, the polar angle θ_b and the azimuthal angle ϕ_b of l^- from the \bar{t} decay are defined in the \bar{t} rest frame $F_{\bar{t}}$ constructed by boosting the tt center of mass frame F_0 along the anti-top quark momentum direction. Through the present work, it is important to keep in mind that the three coordinate systems F_0 , F_t and $F_{\bar{t}}$ have parallel directions of coordinate axes. Note that the polarization efficiency is unity in the semileptonic decays, implying that the charged lepton analyzes the spin of the top quark much more efficiently than the corresponding b quark.

To lowest order in the SM and in the narrow-width approximation we obtain the following normalized distribution of the semileptonic t decay:

$$N(t; \bar{b}l)_0 = \frac{12x(1-x)}{(1+2w)(1-w)^2} D_t^{\frac{1}{2}}(\theta_1^i) dx \frac{d\phi_1}{4}; \tag{30}$$

$$N(t; b\bar{l})_0 = \frac{12x(1-x)}{(1+2w)(1-w)^2} D_{\bar{t}}^{\frac{1}{2}}(\theta_b^i) dx \frac{d\phi_b}{4}; \tag{31}$$

where θ_1^i and θ_b^i refer to the helicities of the t and \bar{t} , respectively, and

$$\begin{aligned}
x &= \frac{2E_l}{m_t}; \quad x = \frac{2E_{\bar{l}}}{m_t}; \quad w = \frac{m_W^2}{m_t^2}; \quad w < x(x) < 1; \\
d\phi_1 &= d\phi_1 d\phi_b; \quad d\phi_b = d\phi_1 d\phi_b;
\end{aligned} \tag{32}$$

The factorization of the lepton distribution into an energy and angular dependent part holds and this property is irrespective of whether the W boson is on-shell or not. It was shown in Ref. [16] that even the order s QCD corrections respect this factorization property to a high degree of accuracy.

3.3 CP-odd observables

The differential cross section of the process $e^+e^- \rightarrow t\bar{t}$, followed by the decays $t \rightarrow bX^+$ and $\bar{t} \rightarrow \bar{b}X^-$ is given by

$$\frac{d\sigma}{d\Omega} (e^+e^- \rightarrow t\bar{t} \rightarrow bX^+ \bar{b}X^-)_{L,R} = \frac{6}{s} B_X^+ B_X^- \left[\frac{d\cos\theta}{4} \frac{d\phi}{4} \right] \quad (33)$$

where for notational convenience the abbreviations

$$\begin{aligned} \cos\theta_1 &= \sin\theta \cos\phi; & \cos\theta_2 &= \sin\theta \sin\phi; & \cos\theta_3 &= \cos\theta; \\ \cos\phi_1 &= \sin\theta \cos\phi; & \cos\phi_2 &= \sin\theta \sin\phi; & \cos\phi_3 &= \cos\theta; \end{aligned} \quad (34)$$

are used, θ is the scattering angle between the electron and top-quark momenta, and B_X^+ and B_X^- are the branching fractions of $t \rightarrow bX^+$ and $\bar{t} \rightarrow \bar{b}X^-$. Here, the angular dependence $_{L,R}$ is given by

$$_{L,R} (\cos\theta_1 \cos\theta_2 \cos\theta_3) = \sum_{\alpha=0}^X M_{\alpha}^{L,R} M_{\alpha}^{L,R} D_{\alpha}^X \cos\theta_1 \cos\theta_2 \cos\theta_3 \quad (35)$$

In the e^+e^- cm frame the angular dependence $_{L,R}$ for the process $e^+e^- \rightarrow t\bar{t} \rightarrow (X^+b)(X^- \bar{b})$ can be written as

$$\begin{aligned} _{L,R} (\cos\theta_1 \cos\theta_2 \cos\theta_3) &= P_{1L,R} D_1 + P_{2L,R} D_2 \\ &+ \frac{(\cos\theta_1 + \cos\theta_2)}{2} P_{3L,R} + \frac{(\cos\theta_1 - \cos\theta_2)}{2} P_{4L,R} D_3 + \frac{(\cos\theta_1 + \cos\theta_3)}{2} P_{4L,R} + \frac{(\cos\theta_1 - \cos\theta_3)}{2} P_{3L,R} D_4 \\ &+ \frac{(\cos\theta_2 + \cos\theta_3)}{2} P_{5L,R} + \frac{(\cos\theta_2 - \cos\theta_3)}{2} P_{6L,R} D_5 + \frac{(\cos\theta_2 + \cos\theta_1)}{2} P_{6L,R} + \frac{(\cos\theta_2 - \cos\theta_1)}{2} P_{5L,R} D_6 \\ &+ \frac{(\cos\theta_3 + \cos\theta_1)}{2} P_{7L,R} + \frac{(\cos\theta_3 - \cos\theta_1)}{2} P_{8L,R} D_7 + \frac{(\cos\theta_3 + \cos\theta_2)}{2} P_{8L,R} + \frac{(\cos\theta_3 - \cos\theta_2)}{2} P_{7L,R} D_8 \\ &+ \sum_{\alpha=9}^{16} P_{\alpha L,R} D_{\alpha} \quad ; \end{aligned} \quad (36)$$

where the definition of the sixteen (16) functions P_X ($X = L, R$) and the sixteen correlation functions D_{α} ($\alpha = 1$ to 16) is given in Appendices A and B, respectively, and $(\cos\theta) = \cos\theta_w$ for the inclusive $t(\bar{t})$ decay and unity for the semileptonic $t(\bar{t})$ decay.

The terms P_{α} and D_{α} can thus be divided into four categories under CP and CPT: even-even, even-odd, odd-even, and odd-odd terms. CP-odd coefficients directly measure CP

violation and $CP\bar{T}$ -odd terms indicate rescattering effects. Table 1 shows that there exist six (6) independent CP -odd terms among which P_5, P_{12}, P_{14} and P_3 are $CP\bar{T}$ -even, and P_3, P_7 and P_{16} $CP\bar{T}$ -odd.

From now on we make a detailed investigation of the production process $e^+e^- \rightarrow t\bar{t}$. Recently, CP violation in the production process has been extensively investigated. Here, we study the CP -violating effects of the process $e^+e^- \rightarrow t\bar{t}$ in a rather unified manner. As shown previously, we can consider three CP -odd and $CP\bar{T}$ -even and three CP -odd and $CP\bar{T}$ -odd terms.

Including electron beam polarization, we can obtain thirty-two (32) observables in total:

$$32 = \underset{\text{Electron Pol:}}{\underset{*}{2}} \underset{t \text{ and } \bar{t} \text{ Pol:}}{\underset{*}{(2-2)^2}}$$

Here, the first 2 is for the electron helicity, and two 2's in the parentheses for the degrees of top and anti-top polarizations. It is therefore clear that the classification according to the CP and $CP\bar{T}$ transformation properties gives us a complete set of observables that can be measured in the process $e^+e^- \rightarrow t\bar{t}$ with left- and right-handed polarized electron beams.

The CP -odd part of the angular dependence (36) can be separated into two parts

$$\underset{L,R}{CP}(\theta; \phi_1; \phi_2; \phi_3; \phi_4) = \underset{EL,R}{CP} + \underset{OL,R}{CP}; \quad (37)$$

where $\underset{EL,R}{CP}$ and $\underset{OL,R}{CP}$ terms are $CP\bar{T}$ -even and $CP\bar{T}$ -odd, respectively, and given by

$$\underset{EL,R}{CP} = P_{5L,R} \left[\frac{(\cos\theta + 1)}{2} D_5 + \frac{(\cos\theta - 1)}{2} D_6 \right] + [P_{12L,R} D_{12} + P_{14L,R} D_{14}]; \quad (38)$$

$$\begin{aligned} \underset{OL,R}{CP} = & P_{3L,R} \left[\frac{(\cos\theta + 1)}{2} D_3 + \frac{(\cos\theta - 1)}{2} D_4 \right] + P_{7L,R} \left[\frac{(\cos\theta + 1)}{2} D_7 + \frac{(\cos\theta - 1)}{2} D_8 \right] \\ & + P_{16} D_{16}; \end{aligned} \quad (39)$$

The explicit form of all the CP -odd terms is listed in Appendix A. The upper three CP -odd P_X terms are $CP\bar{T}$ -even and the lower three CP -odd terms are $CP\bar{T}$ -odd.

Including electron beam polarization, Poulse and Rindani[10] recently have considered two new CP -odd and $CP\bar{T}$ -even asymmetries, which are essentially equivalent to the so-called triple vector products, and two new CP -odd and $CP\bar{T}$ -odd asymmetries in addition to the two conventional lepton energy asymmetries. It is clear that we can use six more asymmetries among which four asymmetries are CP -odd and $CP\bar{T}$ -even and the other two terms are CP -odd and $CP\bar{T}$ -odd.

3.4 Top-quark momentum reconstruction

Purely semileptonic decay modes of a $t\bar{t}$ pair also give the cleanest signal for the top-pair production process in e^+e^- collisions:

$$\begin{aligned} e^-(p_e) + e^+(p_{\bar{e}}) &\rightarrow t(p_t) + \bar{t}(p_{\bar{t}}); \\ t(p_t) &\rightarrow b(p_b) + W^+(p_W); \end{aligned}$$

$$\begin{aligned}
t(p_t) &= b(p_b) + W(p_w); \\
W^+(p_w) &= l(p_l) + \bar{\nu}(p); \\
W^-(p_w) &= l(p_l) + \nu(p);
\end{aligned} \tag{40}$$

The process is observed experimentally as shown in Figure 2;

$$e^+ + e^- \rightarrow b + \bar{b} + l + \bar{l} + \text{missing momentum}; \tag{41}$$

where the final lepton pair can be either one of e^+e^- , $e^+\mu^-$, $e^+\tau^-$, $\mu^+\mu^-$, and $\mu^+\tau^-$. The four-momenta of the particles are given in parentheses.

A simple kinematical analysis, presented below, shows that the two unobserved neutrino momenta can be determined from the observed b, \bar{b} , and lepton momenta with no ambiguity, in the limit where the t and W widths and photon (or gluon) radiation are neglected.

The kinematics of the process (40) is determined by ten angles, two for the scattering, four each for the semileptonic t decays. Since we observe the four three-momenta of the final particles, generally we have superfluous observables to fix the whole configuration. Here we present an explicit solution for the two momenta p_w and $p_{\bar{w}}$ in terms of the observed b, \bar{b} , and lepton momenta so that the t and \bar{t} momenta can be reconstructed.

It suffices to solve for the three-momentum \mathbf{p}_w and then $\mathbf{p}_{\bar{w}}$ is given by momentum conservation. As the t energy is equal to the beam energy E , we have

$$p_w^0 = E - p_b^0; \quad \mathbf{p}_w^2 = (E - p_b^0)^2 - m_w^2; \tag{42}$$

A similar equation holds for the $t \rightarrow bW$ decay:

$$\mathbf{p}_{\bar{w}}^2 = (E - p_{\bar{b}}^0)^2 - m_w^2; \tag{43}$$

Using momentum conservation $\mathbf{p}_w = \mathbf{p}_{\bar{w}} + \mathbf{p}_b + \mathbf{p}_{\bar{b}}$ and Eq. (42), this last equation can be written in terms of \mathbf{p}_w :

$$(\mathbf{p}_b + \mathbf{p}_{\bar{b}}) \cdot \mathbf{p}_w = E(p_b^0 - p_{\bar{b}}^0) - p_b^0 p_{\bar{b}}^0 + m_b^2 - m_{\bar{b}}^2; \tag{44}$$

The third constraint comes from the condition that the bW^+ system should have the mass of the t quark:

$$(\mathbf{p}_b + \mathbf{p}_w)^2 = m_t^2; \tag{45}$$

which gives

$$\mathbf{p}_b \cdot \mathbf{p}_w = E p_b^0 - p_b^0 p_w^0 + \frac{1}{2}(m_w^2 + m_b^2 - m_t^2); \tag{46}$$

Eqs. (44) and (46) lead to

$$\mathbf{p}_b \cdot \mathbf{p}_w = E p_b^0 - p_b^0 p_w^0 + \frac{1}{2}(m_t^2 + m_b^2 - m_w^2); \tag{47}$$

The sequential $W^+ \rightarrow l^+ \bar{\nu}_l$ decay yields another condition:

$$(\mathbf{p}_W - \mathbf{p}_l)^2 = 0; \quad (48)$$

which gives

$$\mathbf{p}_1 \cdot \mathbf{p}_W = E \mathbf{p}_1^0 - \mathbf{p}_1^0 p_1^0 = \frac{1}{2} (m_W^2 + m_l^2); \quad (49)$$

The four conditions (42), (46), (47), and (49) provide the solution for \mathbf{p}_W . We rewrite the right-hand sides of these equations for the sake of clarity:

$$\mathbf{p}_W^2 = K; \quad \mathbf{p}_b \cdot \mathbf{p}_W = L; \quad \mathbf{p}_{\bar{b}} \cdot \mathbf{p}_W = M; \quad \mathbf{p}_1 \cdot \mathbf{p}_W = N; \quad (50)$$

Let us assume, for the moment, that the three momenta \mathbf{p}_b , $\mathbf{p}_{\bar{b}}$ and \mathbf{p}_1 are not parallel. Then we can expand \mathbf{p}_W in terms of any combination of two momenta among the three momenta. Here, we choose \mathbf{p}_b and $\mathbf{p}_{\bar{b}}$, for which \mathbf{p}_W is expressed as

$$\mathbf{p}_W = a\mathbf{p}_b + b\mathbf{p}_{\bar{b}} + c\mathbf{p}_1; \quad (51)$$

The second and third expressions in Eq. (50) constrain \mathbf{p}_W to lie on a line in three-dimensional space. They give

$$\begin{aligned} a\mathbf{p}_b^2 + b\mathbf{p}_{\bar{b}}^2 &= L; \\ a\mathbf{p}_b \cdot \mathbf{p}_{\bar{b}} + b\mathbf{p}_{\bar{b}}^2 &= M; \end{aligned} \quad (52)$$

which can be explicitly solved:

$$\frac{a}{b} = \frac{1}{\mathbf{p}_b \cdot \mathbf{p}_{\bar{b}}} \frac{\mathbf{p}_b^2}{\mathbf{p}_{\bar{b}}^2} \frac{L}{M}; \quad (53)$$

The remaining variable c is determined using the final two conditions of Eq. (50):

$$c^2 = \frac{1}{\mathbf{p}_b \cdot \mathbf{p}_{\bar{b}}} K - a^2 \mathbf{p}_b^2 - b^2 \mathbf{p}_{\bar{b}}^2 - 2ab\mathbf{p}_b \cdot \mathbf{p}_{\bar{b}}; \quad (54)$$

$$c = \frac{1}{\mathbf{p}_1 \cdot (\mathbf{p}_b \times \mathbf{p}_{\bar{b}})} N - a\mathbf{p}_1 \cdot \mathbf{p}_b - b\mathbf{p}_1 \cdot \mathbf{p}_{\bar{b}}; \quad (55)$$

The sign of c can not be determined by the first equation, but this twofold discrete ambiguity is cleared out through the second constraint which stems from the extra information on the antilepton momentum.

There are two exceptional cases where the t and \bar{t} momenta can not be determined. (i) In the exceptional case that two momenta are parallel, one has a twofold discrete ambiguity, and (ii) in the more exceptional case that three momenta are parallel, one obtains an one-parameter family of solution for which the azimuthal angle of \mathbf{p}_W with respect to \mathbf{P}_b is left undetermined. Even from experimental point of view such two cases are so exceptional that the reconstruction of the t and \bar{t} momenta can be almost always possible.

3.5 CP-odd observables in the laboratory frame

Experimentally it is, however, difficult to perform a 16-parameter fit (corresponding to the 16 angular coefficients) for each of several $\cos\theta$ bins. Rather one would like to obtain from the experimental data the moments of those angular distributions that are most sensitive to new physics, i.e. the anomalous CP-violating form factors, c and c_z at hand. However, a sufficiently precise reconstruction of the top quark direction is required to measure all the angular variables. The reconstruction is easy if either the top quark or the top anti-quark decays into a b quark and W boson that decays hadronically. We have shown in Section 3.4 that in the process $e^+e^- \rightarrow t\bar{t}$ even the purely semileptonic decays of the t and \bar{t} quarks allow the full reconstruction of the particle momenta, especially the top and anti-top momenta. In practice, the use of the directly measurable momenta of the charged leptons and/or b-jets might be easier. When the top quark and anti-top quark directions are not determined, the cross section should be rewritten in the laboratory frame and variables independent of the top quark and anti-quark directions should be used. These transformations can be straightforwardly performed and several useful angular variables can be introduced.

The previous works have concentrated on the CP-odd observables expressed in terms of the directly measurable particle momenta. However, the analytic expressions of those observables are very much involved even if the CP-odd terms for the specific and the helicity values are very simple.

First of all we investigate the kinematics of the production-decay sequence

$$e^+e^- \rightarrow t\bar{t} \rightarrow X^+bX^-b \quad (56)$$

The t and \bar{t} momenta are, of course, back to back. The b and \bar{b} momenta can be measured. In the laboratory frame, the momenta of X^+ ($q_X; \theta; \phi$) and X^- ($q_X; \theta; \phi$) are referred with respect to the direction of the top quark. The boosts between the laboratory frame and each of the top and anti-top rest frames are defined by the parameters $\gamma = \frac{E}{m_t} = \frac{1}{\sqrt{1-\beta^2}}$ and $\beta = \frac{p}{E} = \frac{p}{m_t \gamma}$. The momentum variables between the laboratory frame and the top rest frame are related by

$$\begin{aligned} E_X &= (E_X + q_X \cos \theta); & \phi' &= \phi; \\ q_X \cos \theta &= (q_X \cos \theta + E_X); & q_X \sin \theta &= q_X \sin \theta; \end{aligned} \quad (57)$$

and those between the laboratory frame and the anti-top rest frame are related by

$$\begin{aligned} E_X &= (E_X - q_X \cos \theta); & \phi' &= \phi; \\ q_X \cos \theta &= (q_X \cos \theta - E_X); & q_X \sin \theta &= q_X \sin \theta; \end{aligned} \quad (58)$$

Observables which are constructed from the (unit) momenta of the charged leptons and/or b jets originating from t and \bar{t} decay are directly measurable in future experiments. Both the nonleptonic and semileptonic decay channels

$$t \rightarrow bX_{\text{had}}; \quad (59)$$

$$t \rightarrow b\ell^+; \quad \ell = e, \mu, \tau; \quad (60)$$

together with the corresponding charge-conjugated ones are used in the following. The first set of observables which we consider involves the momentum of a lepton or b jet from t decay

correlated with the momentum of a lepton or b jet from t decay. These correlations apply to the reactions

$$e^+ (p_e) + e^- (p_e) \rightarrow t + \bar{t} \rightarrow a(q_+) + c(q_-) + X; \quad (61)$$

where we use the notation $a; c = e^+; \mu^+; \tau^+; b$ jet, and $a; c$ will denote the corresponding charge conjugate particles. The momenta p_e and q are defined in the overall c.m. frame. Light quark jets resulting from the hadronic decays are difficult to identify and are therefore not used for constructing observables in the following. We shall assume that the momentum is measurable with a suitable vertex chamber. The subsequent analysis holds for all reactions of the form irrespectively of the intermediate $t\bar{t}$ state and of the unobserved part X of the final state.

Let us start with the CP-odd energy asymmetries

$$A_E^b = E_b - E_{\bar{b}}; \quad A_E^1 = E_1 - E_{\bar{1}}; \quad (62)$$

The CP-odd asymmetries are proportional to the CP-T-odd correlation function D_7 :

$$A_E^b = \frac{r}{3} E_b D_7; \quad \langle A_E^1 \rangle = \frac{r}{3} \langle E_1 \rangle D_7; \quad (63)$$

where $E_b = (m_t^2 - m_W^2)/2m_t$ and the notation $\langle \dots \rangle$ denotes the average of the observable X over the lepton energy distribution. Explicitly we obtain for the average of the lepton energy

$$\langle E_1 \rangle = \frac{m_t}{2} \int_0^1 dx \frac{6x^2(1-x)}{(1+2w)(1-w)^2} = \frac{m_t}{4} \frac{1+2w+3w^2}{1+2w}; \quad (64)$$

with w defined in Equation (32), and for the expectations of the CP-odd energy asymmetries

$$\begin{aligned} \langle A_E^b \rangle &= \frac{4}{9} E_b^2 \frac{1}{w} v_{L,R} \text{Im}(c_{L,R}); \\ \langle A_E^1 \rangle &= \frac{4}{9} \langle E_1 \rangle^2 v_{L,R} \text{Im}(c_{L,R}); \end{aligned} \quad (65)$$

Secondly, let us investigate the CP-odd vector observables

$$A_1^b = \hat{p}_e \cdot (\hat{p}_a - \hat{p}_b); \quad A_2^b = \hat{p}_e \cdot (\hat{p}_+ - \hat{p}_b); \quad (66)$$

$$A_1^1 = \hat{p}_e \cdot (\hat{p}_a - \hat{p}_1); \quad A_2^1 = \hat{p}_e \cdot (\hat{p}_+ - \hat{p}_1); \quad (67)$$

The four CP-odd vector observables can be expressed in the t and \bar{t} rest frames in terms of the angular correlations D_i ($i = 1$ to 16) defined in Appendix B, as

$$\begin{aligned} A_1^b &= \frac{r}{3} E_b^2 \cos D_{12} - \sin D_{14} \frac{r}{3} \sin D_5; \\ A_2^b &= \frac{r}{3} E_b^2 \cos D_7 - \sin D_3; \end{aligned} \quad (68)$$

$$\begin{aligned} \langle A_1^1 \rangle &= \frac{r}{3} \langle E_1 \rangle^2 \cos D_{12} - \sin D_{14} + \frac{r}{3} \sin D_5; \\ \langle A_2^1 \rangle &= \frac{r}{3} \langle E_1 \rangle^2 \cos D_7 - \sin D_3; \end{aligned} \quad (69)$$

It is now straightforward to obtain the analytic expressions for the expectation of the observables O_i^X ($= A_i^b; hA_{iE}^1$) ($X = b; 1$ and $i = 1; 2$) defined by

$$hO_i^X = \frac{1}{2} \frac{1}{(4)^2} \int_0^{\pi} \int_0^{2\pi} d\cos\theta \, d\phi \, O_i^X(\theta; \phi; \theta_1; \phi_1; \theta_2; \phi_2; \theta_3; \phi_3); \quad (70)$$

where $d = d\cos\theta$ and $d = d\cos\theta$. We obtain for the expectations of the CP-odd vector observables

$$\begin{aligned} hA_{1L,R}^b &= \frac{4}{27} E_b^2 \left(\frac{2}{3} v_{L,R} + a_{L,R} \operatorname{Re}(c_{L,R}) \right); \\ hA_{2L,R}^b &= \frac{4}{9} E_b^2 \left(\frac{2}{3} a_{L,R} \operatorname{Im}(c_{L,R}) \right); \\ hA_{1E}^1 h_{L,R} &= \frac{4}{27} hE_{1E}^2 \left(\frac{2}{3} v_{L,R} + a_{L,R} \operatorname{Re}(c_{L,R}) \right); \\ hA_{2E}^1 h_{L,R} &= \frac{4}{9} hE_{1E}^2 \left(\frac{2}{3} a_{L,R} \operatorname{Im}(c_{L,R}) \right); \end{aligned} \quad (71)$$

Thirdly, we turn to the CP-odd tensor observables and take $i; j = 3$ to consider the (3;3) components with respect to the electron momentum direction

$$\begin{aligned} T_{33}^b &= 2(\mathbf{p}_b \cdot \mathbf{p}_b)(\mathbf{p}_b \cdot \mathbf{p}_b); \\ Q_{33}^b &= 2(\mathbf{p}_b + \mathbf{p}_b)(\mathbf{p}_b \cdot \mathbf{p}_b) - \frac{2}{3}(\mathbf{p}_b^2 \cdot \mathbf{p}_b^2); \end{aligned} \quad (72)$$

$$\begin{aligned} T_{33}^1 &= 2(\mathbf{p}_1 \cdot \mathbf{p}_1)(\mathbf{p}_1 \cdot \mathbf{p}_1); \\ Q_{33}^1 &= 2(\mathbf{p}_1 + \mathbf{p}_1)(\mathbf{p}_1 \cdot \mathbf{p}_1) - \frac{2}{3}(\mathbf{p}_1^2 \cdot \mathbf{p}_1^2); \end{aligned} \quad (73)$$

The four CP-odd tensor observables can be expressed in the t and t rest frames in terms of the angular correlations D ($= 1$ to 16) and some extra angular correlations D^0 ($= 1$ to 12), which are defined in Appendix B, as

$$\begin{aligned} T_{33}^b &= \frac{2}{9} E_b^2 \left(\frac{2}{3} (2 + 1) D_5 + 9 D_{14} \sin\theta \cos\theta \right. \\ &\quad \left. + 3 (3 \cos^2\theta - 1) D_{12} \right) \\ &\quad + \frac{2}{15} E_b^2 \left(\frac{2}{3} D_4^0 + D_6^0 + \frac{2}{3} (2 + 1) D_8^0 \right. \\ &\quad \left. D_7^0 + 2 D_9^0 \sin\theta \cos\theta + (D_{11}^0 + \frac{2}{3} D_3^0) \sin^2\theta \right. \\ &\quad \left. + \cos^2\theta D_{10}^0 + (2 \cos^2\theta - 1) D_{11}^0 \right); \\ Q_{33}^b &= \frac{4}{9} E_b^2 \left(3 \sin\theta \cos\theta D_3 + (3 \cos^2\theta - 1) D_7 \right. \\ &\quad \left. + \frac{2}{15} E_b^2 \frac{1}{3} (2 + 1) (3 \cos^2\theta - 1) D_1^0 + \frac{2}{3} \sin^2\theta D_2^0 \right) \end{aligned}$$

$$\begin{aligned}
& + 2 \frac{P}{3} \sin \cos D \frac{0}{5} ; \\
h\Gamma_{33}^1 i_E &= \frac{2}{9} \frac{P}{2} hE_1^2 i_E f 7 \frac{P}{3} (2^2 - 1) D_5 - 9^2 D_{14} g \sin \cos \\
& + 3 (3 \cos^2 - 1) D_{12} \\
& + \frac{2}{15} \frac{P}{10} hE_1^2 i_E \left(\frac{P}{3} 2^2 D_4^0 - D_6^0 - \frac{P}{3} (2^2 + 1) D_8^0 \right. \\
& + D_7^0 - 2 D_9^0 \sin \cos + (D_{12}^0 - \frac{P}{3} D_3^0) \sin^2 \\
& \left. \cos^2 D_{10}^0 + (2 \cos^2 - 1) D_{11}^0 \right) ; \\
hQ_{33}^1 i_E &= \frac{4}{9} \frac{P}{6} hE_1^2 i_E - 3 \sin \cos D_3 - (3 \cos^2 - 1) D_7 \\
& + \frac{2}{15} \frac{P}{10} hE_1^2 i_E \frac{1}{3} (2^2 + 1) (3 \cos^2 - 1) D_1^0 - \frac{P}{3} \sin^2 D_2^0 \\
& + 2 \frac{P}{3} \sin \cos D \frac{0}{5} ;
\end{aligned} \tag{74}$$

$$\begin{aligned}
hQ_{33}^1 i_E &= \frac{4}{9} \frac{P}{6} hE_1^2 i_E - 3 \sin \cos D_3 - (3 \cos^2 - 1) D_7 \\
& + \frac{2}{15} \frac{P}{10} hE_1^2 i_E \frac{1}{3} (2^2 + 1) (3 \cos^2 - 1) D_1^0 - \frac{P}{3} \sin^2 D_2^0 \\
& + 2 \frac{P}{3} \sin \cos D \frac{0}{5} ;
\end{aligned} \tag{75}$$

where the average of the lepton energy squared $hE_1^2 i$ is given by

$$hE_1^2 i_E = \frac{m_t^2}{4} \frac{Z}{w} \int_0^1 dx \frac{6x^3(1-x)}{(1+2w)(1-wx)^2} = \frac{3m_t^2}{40} \frac{1+2w+3w^2+4w^3}{1+2w} ; \tag{76}$$

with $w = m_W^2/m_t^2$. We do not present the analytic expressions for the expectation values of the CP-odd tensor observables although they are straightforward to obtain.

3.6 Observable consequences of the top-quark EDM

For the sake of numerical analysis we insert the values of the SM vector and axial-vector couplings and then we obtain

$$\begin{aligned}
v_L &= 0.67 + 0.15 z ; & v_R &= 0.67 - 0.13 z ; \\
a_L &= -0.38 z ; & a_R &= 0.32 z ; \\
c_L &= c + 0.64 z c_z ; & c_R &= c - 0.55 z c_z ;
\end{aligned} \tag{77}$$

where $z = (1 - m_Z^2/s)^{-1}$. The contribution from the Z-boson exchange diagram decreases as the c.m. energy \sqrt{s} increases. For $m_t = 175$ GeV and $m_Z = 91.2$ GeV, $1/z = 1.073$. Note that the c_z contribution to c_L and c_R is similar in size but different in sign. Naturally, the electron polarization is expected to play a crucial role in discriminating c and c_z , as pointed out earlier by Cuyppers and Rindani[9].

If a non-vanishing expectation value $hO_X i$ for a given observable O_X is observed, it has a statistical significance as far as it is compared with the expectation variance $hO_X^2 i$. For instance, to observe a deviation from the SM expectation with better than one-standard deviations one

needs

$$hO_X i = \frac{s}{N_{tt}} \frac{hO_X^2 i}{N_{tt}}; \quad N_{tt} = \epsilon B_X + B_X L_{ee} (e^+ e^- \rightarrow tt); \quad (78)$$

where N_{tt} is the number of events, L_{ee} is the $e^+ e^-$ collider luminosity, and ϵ is the detection efficiency.

Implementing Eq. (78) we can determine the areas in the $(c; c_z)$ plane which can not be explored with a given confidence level. Clearly, because of the linear dependence of the expectation values on the CP-odd electroweak dipole form factors, these areas are delimited by straight lines which are equidistant from the SM expectation $c = c_z = 0$. The slopes of these straight lines vary with the polarization degree of the initial $e^+ e^-$ beams. The use of more than two CP-odd distributions can help to determine independently the real and imaginary parts of the electric as well as weak dipole couplings. Of course, longitudinal beam polarization, if present, obviates the need for the simultaneous measurement of more than one distribution and it can enhance the sensitivity to the CP-odd parameters. Our numerical results are presented for the assumed detection efficiency $\epsilon = 10\%$ and for the following set of experimental parameters:

$$\sqrt{s} = 0.5 \text{ TeV}; \quad L_{ee} = \begin{cases} 10 \text{ fb}^{-1} & \text{for polarized electrons;} \\ 20 \text{ fb}^{-1} & \text{for unpolarized electrons;} \end{cases} \quad (79)$$

The shadowed parts in Figure 3 show the 1- σ allowed regions of the CP-odd parameters $\text{Re}(c)$ and $\text{Re}(c_z)$ through the CP-odd and CP-even asymmetries (a) A_1^b and T_{33}^b and (b) A_1^1 and T_{33}^1 with left- and right-handed polarized electron beams, respectively. The solid lines with a positive (negative) slope are for A_1^b and A_1^1 with right-handed (left-handed) electrons while the long-dashed lines with a positive (negative) slope are for T_{33}^b and T_{33}^1 with right-handed (left-handed) electrons. On the other hand, the shadowed parts in Figure 4 show the 1- σ allowed regions of the parameters $\text{Re}(c)$ and $\text{Re}(c_z)$ through (a) A_1^b and T_{33}^b and (b) A_1^1 and T_{33}^1 with unpolarized electron beams, respectively. The solid lines are for A_1^b and A_1^1 while the long-dashed lines are for T_{33}^b and T_{33}^1 . Two figures present us with several interesting results:

The allowed regions strongly depend on electron polarization. Combining the bounds obtained with left-handed and right-handed electron beams, we obtain very tightly constrained 1- σ regions for $\text{Re}(c)$ and $\text{Re}(c_z)$.

Even with unpolarized electrons and positrons, it is possible to obtain a closed region for the CP-odd parameters by using two or more CP-odd asymmetries. The 1- σ regions become very loose for the parameter $\text{Re}(c)$, but the 1- σ regions for $\text{Re}(c_z)$ remain rather intact.

With polarized electrons, the tightest bound is obtained through the CP-odd vector asymmetry A_1^b in the inclusive top-quark decay mode.

Numerically, the 1- σ allowed region of $\text{Re}(c)$ and $\text{Re}(c_z)$ at the cm. energy $\sqrt{s} = 500 \text{ GeV}$ with the total $e^+ e^-$ integrated luminosity 20 fb^{-1} , which is the sum of the integrated luminosities for left- and right-handed electrons, is

$$|\text{Re}(c)| \leq 0.12; \quad |\text{Re}(c_z)| \leq 0.20; \quad (80)$$

The shadowed parts in Figure 5 show the 1- allowed regions of the CP-odd parameters $\text{Im}(c)$ and $\text{Im}(c_z)$ through the CP-odd and CPT-odd asymmetries (a) A_E^b, A_2^b and Q_{33}^b and (b) A_E^1, A_2^1 and Q_{33}^1 with polarized electron beams, respectively. The solid lines with a positive (negative) slope are for A_E^b and A_2^b with right-handed (left-handed) electrons while the long-dashed lines with a positive (negative) slope are for A_2^1 and A_2^1 with right-handed (left-handed) electrons. And, the dot-dashed lines with a positive (negative) slope are for Q_{33}^b and Q_{33}^1 with right-handed (left-handed) electrons. On the other hand, the shadowed parts in Figure 6 show the 1- allowed regions of the parameters $\text{Im}(c)$ and $\text{Im}(c_z)$ through (a) A_E^b, A_2^b and Q_{33}^b and (b) A_E^1, A_2^1 and Q_{33}^1 with unpolarized electron beams, respectively. The solid lines are for A_E^b and A_2^1 while the long-dashed lines are for A_2^b and A_2^1 . And, the dot-dashed lines are for Q_{33}^b and Q_{33}^1 . Two figures present us with several interesting results:

The allowed regions strongly depend on electron polarization. Combining the bounds obtained with left-handed and right-handed electron beams, we obtain very tightly constrained 1- regions for $\text{Im}(c)$ and $\text{Im}(c_z)$.

Even with unpolarized electrons and positrons, it is possible to obtain a bounded region for the CP-odd parameters by using two or more CP-odd asymmetries. We find that the 1- regions become very loose for the parameter $\text{Im}(c_z)$, but the 1- regions for $\text{Re}(c)$ remain rather intact.

With polarized electrons, the tightest bound is obtained through the CP-odd energy asymmetry A_E^b in the inclusive top-quark decay mode.

Numerically, the 1- allowed region of the parameters $\text{Im}(c)$ and $\text{Im}(c_z)$ with the total e^+e^- integrated luminosity 20 fb^{-1} at the cm. energy $\sqrt{s} = 500 \text{ GeV}$ is

$$|\text{Im}(c)| \leq 0.16; \quad |\text{Im}(c_z)| \leq 0.27; \quad (81)$$

4 Compton backscattered laser light

Let us describe in a general framework how photon polarization can provide us with an efficient mechanism [17] to probe CP invariance in the two-photon mode. With purely linearly-polarized photon beams, we classify all the distributions according to their CP and CPT properties. Then, we show explicitly how linearly polarized photon beams allow us to construct two CP-odd and CPT-even asymmetries which do not require detailed information on the momenta and polarizations of the final-state particles.

4.1 Formalism

Generally, a purely polarized photon beam state is a linear combination of two helicity states and the photon polarization vector can be expressed in terms of two angles θ and ϕ in a given coordinate system as

$$|j; i\rangle = \cos(\theta) e^{i\phi} |j; i\rangle + \sin(\theta) e^{i\phi} |j; -i\rangle; \quad (82)$$

where $0 \leq \theta_1 \leq 2\pi$ and $0 \leq \theta_2 \leq 2\pi$. The photon polarization vector (82) implies that the degrees of circular and linear polarization are determined by

$$\langle \sigma \rangle = \cos(2\theta); \quad \langle \tau \rangle = \sin(2\theta); \quad (83)$$

respectively, and the direction of maximal linear polarization is denoted by the azimuthal angle in the given coordinate system. Note that $\langle \sigma \rangle^2 + \langle \tau \rangle^2 = 1$ as expected for a purely polarized photon. For a partially polarized photon beam it is necessary to rescale $\langle \sigma \rangle$ and $\langle \tau \rangle$ by its degree of polarization P ($0 \leq P \leq 1$) as

$$\langle \sigma \rangle = P \cos(2\theta); \quad \langle \tau \rangle = P \sin(2\theta); \quad (84)$$

such that $\langle \sigma \rangle^2 + \langle \tau \rangle^2 = P^2$.

Let us now consider the two-photon system in the c.m. frame where two photon momenta are opposing along the z-axis. The two-photon state vector is

$$\begin{aligned} |j_1; m_1; j_2; m_2\rangle &= |j_1; m_1\rangle |j_2; m_2\rangle \\ &= \cos(\theta_1) \cos(\theta_2) e^{i(j_1 - m_1)\phi_1 + i(j_2 - m_2)\phi_2} \\ &\quad \sin(\theta_1) \cos(\theta_2) e^{i(j_1 + m_1)\phi_1 + i(j_2 - m_2)\phi_2} \\ &\quad \sin(\theta_1) \sin(\theta_2) e^{i(j_1 - m_1)\phi_1 + i(j_2 + m_2)\phi_2} \\ &\quad \cos(\theta_1) \sin(\theta_2) e^{i(j_1 + m_1)\phi_1 + i(j_2 + m_2)\phi_2}; \end{aligned} \quad (85)$$

and then the transition amplitude from the polarized two-photon state to a final state X is simply given by

$$\langle X | \mathcal{M} | j_1; m_1; j_2; m_2 \rangle \quad (86)$$

The azimuthal angles ϕ_1 and ϕ_2 are the directions of maximal linear polarization of the two photons, respectively, in a common coordinate system (For instance, see Figure 7.). In the process $e^+e^- \rightarrow \mu^+\mu^-$, the scattering plane is taken to be the x-z plane in the actual calculation of the helicity amplitudes. The maximal linear polarization angles are then chosen as follows. The angle θ_1 (θ_2) is the azimuthal angle of the maximal linear polarization of the photon beam, whose momentum is in the positive (negative) z direction, with respect to the direction of the momentum in the process $e^+e^- \rightarrow \mu^+\mu^-$. Note that we have used $|j_2; m_2\rangle$ in Eq. (85) for the photon whose momentum is along the negative z direction in order to employ a common coordinate system for the two-photon system.

For later convenience we introduce the abbreviation

$$M_{j_1 j_2} = \langle X | \mathcal{M} | j_1 j_2 \rangle; \quad (87)$$

and two angular variables:

$$\theta = \theta_1 = \theta_2; \quad \phi = \phi_1 + \phi_2; \quad (88)$$

where $0 \leq \theta \leq \pi/2$ and $0 \leq \phi \leq 4\pi$ for a fixed X . It should be noted that (i) the azimuthal angle difference, ϕ , is independent of the final state, while the azimuthal angle sum, ϕ , depends on the scattering plane, and (ii) both angles are invariant with respect to the Lorentz boost along the two-photon beam direction.

It is straightforward to obtain the angular dependence of the σ_X cross section on the initial beam polarizations in terms of the Stokes parameters ($S_1; S_2$) for the degrees of circular polarization and ($S_1; S_2$) for those of linear polarization of the two initial photon beams, respectively, as

$$(S_1; S_2; S_1; S_2) = \sum_X \frac{1}{4} [M_{++}^X + M_{+-}^X + M_{-+}^X + M_{--}^X] \quad (89)$$

where the summation over X is for the polarizations of the final states. Incidentally, the Stokes parameters are expressed in terms of two parameters θ_1 and θ_2 by

$$\begin{aligned} S_1 &= P \cos(2\theta_1); & S_2 &= P \sin(2\theta_1); \\ S_3 &= P \cos(2\theta_2); & S_4 &= P \sin(2\theta_2); \end{aligned} \quad (90)$$

where P and P ($0 \leq P \leq 1$) are the polarization degrees of the two colliding photons. There exist sixteen independent terms, all of which are all measurable in polarized two-photon collisions. Purely linearly polarized photon beams allow us to determine nine terms among all the sixteen terms, while purely circularly polarized photon beams allow us to determine only four terms. The unpolarized cross section is determined in both cases. However, both circular and linear polarizations are needed to determine the remaining four terms.

Even though we obtain more information with both circularly and linearly polarized beams, we study mainly the case where two photons are linearly polarized but not circularly polarized. The expression of the angular dependence then greatly simplifies to

$$\begin{aligned} D(\theta_1; \theta_2; \theta_1; \theta_2) &= \text{unpol} \frac{1}{2} [\cos(\theta_1 + \theta_2) + \cos(\theta_1 - \theta_2)] \langle \sigma_2 \rangle \\ &+ \frac{1}{2} [\sin(\theta_1 + \theta_2) - \sin(\theta_1 - \theta_2)] \langle \sigma_2 \rangle + \frac{1}{2} [\cos(\theta_1 + \theta_2) - \cos(\theta_1 - \theta_2)] \langle \sigma_2 \rangle \\ &+ \frac{1}{2} [\sin(\theta_1 + \theta_2) + \sin(\theta_1 - \theta_2)] \langle \sigma_2 \rangle + \cos(2\theta_1) \langle \sigma_{22} \rangle + \sin(2\theta_1) \langle \sigma_{22} \rangle \\ &+ \cos(2\theta_2) \langle \sigma_{00} \rangle + \sin(2\theta_2) \langle \sigma_{00} \rangle; \end{aligned} \quad (91)$$

where the invariant functions are defined as

$$\begin{aligned} \text{unpol} &= \frac{1}{4} \sum_X M_{++}^X + M_{+-}^X + M_{-+}^X + M_{--}^X \\ \sigma_2 &= \frac{1}{2} \sum_X M_{++}^X (M_{+-}^X + M_{-+}^X) + (M_{+-}^X + M_{-+}^X) M_{--}^X \\ \sigma_2 &= \frac{1}{2} \sum_X M_{++}^X (M_{+-}^X - M_{-+}^X) - (M_{+-}^X - M_{-+}^X) M_{--}^X \\ \sigma_{22} &= \frac{1}{2} \sum_X (M_{+-}^X - M_{-+}^X); & \sigma_{00} &= \frac{1}{2} \sum_X (M_{++}^X - M_{--}^X); \end{aligned} \quad (92)$$

with the subscripts, 0 and 2, representing the magnitude of the sum of two photon helicities of the initial two-photon system.

4.2 Symmetry properties

It is useful to classify the invariant functions according to their transformation properties under the discrete symmetries, CP and CPT [18]. We find that CP invariance leads to the relations

$$\begin{aligned} \sum_X M_{12}^X M_{12}^{X*} &= \sum_X M_{21}^X M_{21}^{X*}; \\ d(\dots) &= d(\dots); \end{aligned} \quad (93)$$

and, if there are no absorptive parts in the amplitudes, CPT invariance leads to the relations

$$\begin{aligned} \sum_X M_{12}^X M_{12}^{X*} &= \sum_X M_{21}^X M_{21}^{X*}; \\ d(\dots) &= d(\dots); \end{aligned} \quad (94)$$

The nine invariant functions in Eq. (91) can then be divided into four categories under CP and CPT: even-even, even-odd, odd-even, and odd-odd terms as in Table 2. CP-odd coefficients directly measure CP violation and CPT-odd terms indicate rescattering effects (absorptive parts in the scattering amplitudes). Table 2 shows that there exist three CP-odd functions; $\text{Re}(\dots)$, $\text{Im}(\dots)$ and $\text{Im}(\dots)$. Here, Re and Im are for real and imaginary parts, respectively. While the first two terms are CPT-even, the last term $\text{Im}(\dots)$ is CPT-odd. Since the CPT-odd term $\text{Im}(\dots)$ requires the absorptive part in the amplitude, it is generally expected to be smaller in magnitude than the CPT-even terms. We therefore study the two CP-odd and CPT-even distributions; $\text{Re}(\dots)$ and $\text{Im}(\dots)$.

We can define two CP-odd asymmetries from the two distributions, $\text{Re}(\dots)$ and $\text{Im}(\dots)$. First, we note that the $\text{Re}(\dots)$ term does not depend on the azimuthal angle whereas the $\text{Im}(\dots)$ does. In order to improve the observability we may integrate the $\text{Re}(\dots)$ term over the azimuthal angle with an appropriate weight function. Without any loss of generality we can take $\text{Re}(\dots)$. Then, the quantity $\text{Re}(\dots)$ in Eq. (91) can be separated by taking the difference of the distributions at $\phi = 0$ and $\phi = \pi$ and the $\text{Im}(\dots)$ by taking the difference of the distributions at $\phi = 0$ and $\phi = \pi$. As a result we obtain the following two integrated CP-odd asymmetries:

$$\hat{A}_{02} = \frac{2}{\text{unpol}} \frac{\text{Re}(\dots)}{\text{unpol}}; \quad \hat{A}_{00} = \frac{\text{Im}(\dots)}{\text{unpol}}; \quad (95)$$

where the factor (2) in the \hat{A}_{02} stems from taking the average over the azimuthal angle with the weight function $\text{sign}(\cos \phi)$:

$$\hat{A}_{02} = \frac{\int_0^{2\pi} d\phi \text{sign}(\cos \phi) \frac{d}{d\phi}}{\int_0^{2\pi} d\phi \frac{d}{d\phi}} = \frac{\int_0^{\pi} d\phi \frac{d}{d\phi} - \int_{\pi}^{2\pi} d\phi \frac{d}{d\phi}}{\int_0^{2\pi} d\phi \frac{d}{d\phi}}; \quad (96)$$

$$\hat{A}_{00} = \frac{\int_0^{2\pi} d\phi \frac{d}{d\phi}}{\int_0^{2\pi} d\phi \frac{d}{d\phi}} = \frac{\int_0^{\pi} d\phi \frac{d}{d\phi} + \int_{\pi}^{2\pi} d\phi \frac{d}{d\phi}}{\int_0^{2\pi} d\phi \frac{d}{d\phi}}; \quad (97)$$

In pair production processes such as $\gamma\gamma \rightarrow e^+e^-$, all the distributions, \mathcal{P}_i , can be integrated over the scattering angle θ with a C P -even angular cut so as to test C P violation.

4.3 Photon spectrum

Recently, the well-known Compton backscattering [19] has drawn a lot of interest because it can be utilized as a powerful high-energy photon source at NLC experiments. In this section we give a detailed description of the energy spectrum and polarization of the Compton backscattered laser lights off high energy electrons or positrons.

We are interested in the situation where a purely linearly polarized laser beam of frequency ω_0 is focused upon an unpolarized electron or positron beam of energy E . In the collision of a laser photon and a linac electron, a high energy photon of energy ω , which is partially linearly polarized, is emitted at a very small angle, along with the scattered electron of energy $E' = E - \omega$. The kinematics of the Compton backscattering process is then characterized by the dimensionless parameters x and y :

$$x = \frac{4E\omega_0}{m_e^2} \approx 15.3 \frac{E}{\text{TeV}} \frac{\omega_0}{\text{eV}}; \quad y = \frac{\omega}{E} \quad (98)$$

In general, the backscattered photon energies increase with x ; the maximum photon energy fraction is given by $y_m = x/(1+x)$. Operation below the threshold [19] for e^+e^- pair production in collisions between the laser beam and the Compton-backscattered photon beam requires $x \geq 2(1+\sqrt{2}) \approx 4.83$; the lower bound on x depends on the lowest available laser frequency and the production threshold of a given final state.

Figure 8(a) shows the photon energy spectrum for various values of x . Clearly large x values are favored to produce highly energetic photons. On the other hand, the degree (y) of linear polarization of the backscattered photon beam reaches the maximum value at $y = y_m$ (See Figure 8(b)),

$$y_{\text{max}} = (y_m) = \frac{2(1+x)}{1+(1+x)^2}; \quad (99)$$

and approaches unity for small values of x . In order to retain large linear polarization we should keep the x value as small as possible.

4.4 Linear polarization transfers

In the two-photon collision case only part of linear polarization of each incident laser beam is transferred to the high-energy photon beam. We introduce two functions, A_0 and A_3 , to denote the degrees of linear polarization transfer [20] as

$$A_0(y) = \frac{h_0(y)}{h_0(y) + 3h_3(y)}; \quad A_3(y) = \frac{h_3(y)}{h_0(y) + 3h_3(y)}; \quad (100)$$

where $h_0(y)$ is the photon energy spectrum function and $h_3(y) = 2y^2 = (x(1-y))^2$ and β is the ratio of the c.m. energy squared \hat{s} to the e^+e^- collider energy squared s . The function A_0 is for the collision of an unpolarized photon beam and a linearly polarized photon beam, and the

function A_{ij} for the collision of two linearly polarized photon beams. The convolution integrals h_{ij} ($i, j = 0, 3$) for a fixed value of θ are defined as

$$h_{ij} = \frac{1}{N^2(x)} \int_{y_{\min}}^{y_{\max}} \frac{dy}{y} \phi_i(y) \phi_j(y); \quad (101)$$

where the normalization factor $N(x)$ is by the integral of the photon energy spectrum ϕ_0 over y .

The event rates of the $\pi^0 \rightarrow \gamma\gamma$ reaction with polarized photons can be obtained by folding a photon luminosity spectral function with the $\pi^0 \rightarrow \gamma\gamma$ production cross section as (for $\theta = 0$)

$$dN_{\pi^0 \rightarrow \gamma\gamma} = dL \cdot d^{\pi^0}(\pi^0 \rightarrow \gamma\gamma); \quad (102)$$

where

$$dL = 2L_{ee} h_{00} dy; \quad (103)$$

$$d^{\pi^0}(\pi^0 \rightarrow \gamma\gamma) = \frac{1}{2s} d_{\pi^0}^{\text{unpol}} \left[A \cos^2 \theta + e^{-i\theta} \right. \\ \left. + A \sin^2 \theta + e^{i\theta} \right] + 2A \cos^2 \theta + e^{-2i\theta} + e^{2i\theta} : \quad (104)$$

Here, α is the e^- conversion coefficient in the Compton backscattering and d_{π^0} is the phase space factor of the final state. The distribution (104) of event rates enables us to construct two CP-odd asymmetries;

$$A_{02} = \frac{2}{N_{\text{unpol}}} \frac{N_{02}}{N_{00}}; \quad A_{00} = \frac{N_{00}}{N_{\text{unpol}}}; \quad (105)$$

where with $y_{\max} = y_m^2$ and $y_{\min} = M_X^2/s$ we have for the event distributions

$$\frac{N_{02}}{N_{00}} = \frac{2L_{ee}}{2s} \frac{1}{y_{\min}} \int_{y_{\min}}^{y_{\max}} \frac{dy}{y} \phi_0(y) \phi_2(y) \quad \frac{N_{00}}{N_{\text{unpol}}} = \frac{2L_{ee}}{2s} \int_{y_{\min}}^{y_{\max}} \frac{dy}{y} \phi_0(y) \phi_0(y) : \quad (106)$$

The asymmetries depend crucially on the two-photon spectrum and the two linear polarization transfers.

We first investigate the \sqrt{s} dependence of the two-photon spectrum and the two linear polarization transfers, A_{02} and A_{00} by varying the value of the dimensionless parameter x . Three values of x are chosen; $x = 0.5, 1$, and 4.83 . Two figures in Figure 9 clearly show that the energy of two photons reaches higher ends for larger x values but the maximum linear polarization transfers are larger for smaller x values. We also note that A_{02} (solid lines) is larger than A_{00} (dashed lines) in the whole range of \sqrt{s} . We should keep the parameter x as large as possible to reach higher energies. However, larger CP-odd asymmetries can be obtained for smaller x values. Therefore, there should exist a compromised value of x , i.e. the incident laser beam frequency ω_0 for the optimal observability of CP violation. The energy dependence of the subprocess cross section and that of the CP-odd asymmetries are both essential to find the optimal x value.

5 Two-photon mode

In this section we reinvestigate CP violation due to the top-quark EDM in the two-photon mode by extending the previous work [11] and revising its numerical errors.

5.1 Helicity Amplitudes

The process $t\bar{t} \rightarrow \gamma\gamma$ consists of two Feynman diagrams and its helicity amplitudes in the c.m. frame are given by

$$M_{\lambda_1 \lambda_2} = \frac{4 Q_t^2 N_c}{(1 - \cos^2 \theta)} A_{\lambda_1 \lambda_2}^h + (i d_t) B_{\lambda_1 \lambda_2} + (i d_t)^2 C_{\lambda_1 \lambda_2}^i; \quad (107)$$

where θ is the scattering angle between t and a photon, and the top-quark EDM factor d_t is given by

$$d_t = \frac{3 c}{4 m_t} = \frac{3}{4} d_t^{\text{SM}}; \quad (108)$$

The SM contributions $A_{\lambda_1 \lambda_2}^h$ are given by

$$\begin{aligned} A_{\lambda_1 \lambda_2}^h &= \frac{4m_t}{s} (\delta_{\lambda_1 \lambda_2} + \cos \theta); & A_{\lambda_1 \lambda_2}^h &= 0; \\ A_{\lambda_1 \lambda_2}^h &= \frac{4m_t}{s} \sin^2 \theta; & A_{\lambda_1 \lambda_2}^h &= 2 \cos \theta \sin \theta; \end{aligned} \quad (109)$$

the terms $B_{\lambda_1 \lambda_2}$, which are linear in d_t , and the terms $C_{\lambda_1 \lambda_2}^i$, which are quadratic in d_t , are given by

$$\begin{aligned} B_{\lambda_1 \lambda_2} &= 2 \frac{p}{s} \frac{8m_t^2}{s} + \cos \theta \sin^2 \theta; \\ B_{\lambda_1 \lambda_2} &= 4m_t \sin \theta \cos \theta; \\ B_{\lambda_1 \lambda_2} &= 2 \frac{p}{s} \sin^2 \theta; \\ B_{\lambda_1 \lambda_2} &= 0; \end{aligned} \quad (110)$$

and

$$\begin{aligned} C_{\lambda_1 \lambda_2}^i &= 2m_t \frac{p}{s} \frac{4m_t^2}{s} + \cos \theta \sin^2 \theta; \\ C_{\lambda_1 \lambda_2}^i &= 4m_t^2 \sin \theta \cos \theta; \\ C_{\lambda_1 \lambda_2}^i &= 2m_t \frac{p}{s} \sin^2 \theta; \\ C_{\lambda_1 \lambda_2}^i &= \sin \theta \frac{4m_t^2}{s} \cos \theta + (1 - \cos^2 \theta); \end{aligned} \quad (111)$$

where $\lambda_1, \lambda_2 = 0, \pm 1$ are the two-photon and t, \bar{t} helicities, respectively, s is the c.m. energy squared, and $\theta = \arccos \frac{1 - 4m_t^2/s}{1 + 4m_t^2/s}$.

5.2 Differential cross section

In counting experiments where the final polarizations are not analyzed, we measure only the following combinations:

$$\sum_{X_1 X_2} M_{X_1 X_2} M_{X_1 X_2}^* = (eQ_t)^4 \sum_{X_1 X_2} M_{X_1 X_2} M_{X_1 X_2}^* : \quad (112)$$

We then find σ_{unpol} , σ_{02} , σ_{22} , and σ_{00} from Equation (92). The differential cross section for a fixed angle is

$$\begin{aligned} \frac{d^2}{d\cos\theta d\phi}(\theta) &= \frac{e^4 Q_t^4 N_c}{8s(1-\cos^2\theta)^2} \left(\sigma_{\text{unpol}} + \frac{1}{2} \langle \sigma_{02} \rangle + \frac{1}{2} \langle \sigma_{22} \rangle + \frac{1}{2} \langle \sigma_{00} \rangle \right) \\ &+ \frac{1}{2} \langle \sigma_{02} \rangle + \frac{1}{2} \langle \sigma_{22} \rangle + \frac{1}{2} \langle \sigma_{00} \rangle ; \end{aligned} \quad (113)$$

$$\sigma_i = \frac{e^4 Q_t^4}{(1-\cos^2\theta)^2} ; \quad \sigma_{02} = \frac{e^4 Q_t^4}{(1-\cos^2\theta)^2} ; \quad (114)$$

for $i = \text{unpol}, 02, 22$, and 00 .

We first note that all the real parts of the distributions (112) are independent of the anomalous CP-odd form factors c up to linear order

$$\begin{aligned} \sigma_{\text{unpol}} &= \frac{1}{4} (1 + 2\sin^2\theta) \left(1 + \sin^4\theta \right) ; \\ \langle \sigma_{02} \rangle &= \frac{16}{f} \sin^2\theta ; \quad \langle \sigma_{22} \rangle = 0 ; \\ \langle \sigma_{00} \rangle &= \frac{4}{f^2} : \end{aligned} \quad (115)$$

Two CP-odd distributions $\langle \sigma_{02} \rangle$ and $\langle \sigma_{00} \rangle$ have contributions from the CP-odd form factor c and they are given by

$$\langle \sigma_{02} \rangle = 0 ; \quad \langle \sigma_{00} \rangle = \frac{24}{m_t} (1 - \cos^2\theta) \text{Re}(c) : \quad (116)$$

A few comments on the CP-odd distributions are in order.

$\langle \sigma_{02} \rangle$ is zero so that it can not be used to probe CP-violating effects from the real part of the top quark EDM.

$\langle \sigma_{00} \rangle$ is not suppressed at threshold.

The CP-odd distribution $\langle \sigma_{00} \rangle$ has the angular dependence $(1 - \cos^2\theta)$ which becomes largest at the scattering angle $\theta = \pi/2$, where the SM contribution is generally small. We, therefore, expect a large CP-odd asymmetry at $\theta = \pi/2$.

5.3 Observable consequences of the top-quark EDM

The CP-odd distribution \mathcal{P}_{02} is useless in determining the top EDM parameter $\text{Re}(c)$, because it vanishes in the top-pair production via two-photon fusion as shown in Eq. (116). In case of \mathcal{P}_{00} , no spin analysis for the decaying top quarks is required and furthermore even the scattering plane does not need to be identified. Even if one excludes the $e^+e^- \rightarrow \gamma\gamma$ modes of 1%, the remaining 99% of the events can be used to measure \mathcal{P}_{00} .

We present our numerical results for the experimental parameters

$$\sqrt{s} = 0.5 \text{ and } 1.0 \text{ TeV}; \quad \mathcal{L}_{ee} = 20 \text{ fb}^{-1}; \quad (117)$$

The dimensionless parameter x , which depends on the laser frequency ω_0 , is treated as an adjustable parameter. We note that $x = 1$ is the maximally allowed value for the e^- conversion coefficient and it may be as small as $x = 0.1$ if the collider is optimized for the e^+e^- model [19]. All one should note is that the significance of the signal scales as $(\mathcal{L}_{ee}^{-2})^{1/2}$, where \mathcal{L}_{ee} denotes the overall detection efficiency that is different for A_{00} and A_{02} .

The CP-odd integrated asymmetry A_{00} depends linearly on the form factor $\text{Re}(c)$ in the approximation that only the terms linear in the form factor are retained. We present the sensitivities to the form factor by varying the parameter x , i.e. the incident laser beam frequency ω_0 .

Folding the photon luminosity spectrum and integrating the distributions over the polar angle θ , we obtain the x -dependence of available event rates:

$$\frac{N_{\text{unpol}}}{N_{00}} = \mathcal{L}_{ee} \frac{Q_t^4 N_c}{2s} \int_{\theta_{\min}}^{\theta_{\max}} d\theta \frac{1}{1 - (\frac{1}{2} \frac{\hbar \omega_0}{m_t} \cos \theta)^2} A_{00}^{\text{unpol}}; \quad (118)$$

where $\theta_{\max} = (x/(1+x))^2$ and $\theta_{\min} = 4m_t^2/s$. After extracting the top EDM form factor $\text{Re}(c)$ from the asymmetry A_{00} as

$$A_{00} = \text{Re}(c) \tilde{A}_{00}; \quad (119)$$

we obtain the 1- σ allowed sensitivity of the form factor $\text{Re}(c)$

$$M_{\text{ax}}(\text{Re}(c)) = \frac{\sqrt{s}}{\tilde{A}_{00} \sqrt{\mathcal{L}_{ee} N_{\text{unpol}}}}; \quad (120)$$

if no asymmetry is found. Here, \mathcal{L}_{ee} denotes the multiplication of the branching fraction times the experimental detection efficiency. The N_{SD} -upper bound is determined simply by multiplying $M_{\text{ax}}(\text{Re}(c))$ by N_{SD} .

A crucial issue is to find an optimal means for maximizing the denominator in Eq. (120) experimentally. It requires obtaining the smallest possible value of x to make the linear polarization transfer as large as possible. However, the large top-quark mass does not allow x to be very small. For a given cm. energy squared, s , the allowed range of x is given by

$$\frac{2m_t}{\sqrt{s}} \leq x \leq 2(1 + \frac{\sqrt{s}}{2m_t}); \quad (121)$$

Experimentally, the process $e^+e^- \rightarrow W^+W^-$ is the most severe background process against the process $e^+e^- \rightarrow t\bar{t}$. Without a detailed background estimation, we simply take the detection efficiency ϵ to be

$$\epsilon = 10\% ; \quad (122)$$

even though more experimental analyses are required to estimate the efficiency precisely. It would be, however, rather straightforward to include the effects from any experimental cuts and efficiencies in addition to the branching factors discussed above.

Figure 10 shows a very strong x dependence of the $\text{Re}(c)$ upper bound, $\text{Max}(|\text{Re}(c)|)$, at $\sqrt{s} = 0.5$ and 1 TeV, from the asymmetry A_{00} . The solid line is for $\sqrt{s} = 0.5$ TeV and the long-dashed line for $\sqrt{s} = 1$ TeV. The doubling of e^+e^- c.m. energy improves the sensitivity so much and renders the optimal x value smaller than that at $\sqrt{s} = 0.5$ TeV. The x values for the optimal sensitivities and the optimal $1-\epsilon$ sensitivity to the CP-odd parameter $\text{Re}(c)$ for $\sqrt{s} = 0.5$ and 1 TeV are listed in Table 3.

6 Conclusions

Large top-quark mass implies that a top quark can serve as an excellent tool to probe CP violation from new interactions at NLC.

In the production process $e^+e^- \rightarrow t\bar{t}$, followed by the t and \bar{t} decays, CP violation from the T-odd top-quark EDM and WDM can be investigated through the angular correlations of the t and \bar{t} decay products.

We have completely defined all the available CP-odd correlations and have established the relations between a lot of previously suggested CP-odd correlations and the linearly-independent CP-odd correlations. We have fully analyzed the dependence of all the CP-odd observables on the electron beam polarization.

Most CP-odd asymmetries in the process $e^+e^- \rightarrow t\bar{t}$ depend on both the top EDM and the top WDM. Therefore, the separation of two contributions requires introducing electron beam polarization and/or using at least two independent CP-odd observables. We found that electron polarization is quite effective in separating the top-quark EDM and WDM effects.

In the polarized mode, initial CP-odd two-photon polarization configurations allow us to measure the top-quark EDM by counting $t\bar{t}$ pair production events in a straightforward way. Without any direct information on the momenta of the top-quark decay products linearly-polarized laser beams with an adjustable beam energy provide us with a very efficient way of probing the top-quark EDM at a PLC.

The strongest $1-\epsilon$ sensitivity on the top EDM factor $\text{Re}(c)$ for $\sqrt{s} = 500$ GeV in the polarized e^+e^- mode is obtained through the vector asymmetry A_1^b and, numerically, it is $|\text{Re}(c)| \leq 0.13$ for the total e^+e^- integrated luminosity 20 fb^{-1} . On the other hand, the optimal $1-\epsilon$ sensitivity on $\text{Re}(c)$ through the asymmetry A_{00} for $\sqrt{s} = 0.5$ TeV in the polarized two-photon mode is $|\text{Re}(c)| \leq 0.16$. Consequently, the polarized e^+e^- mode and the polarized two-photon mode are competitive in probing CP violation in the top-quark pair production processes. Certainly, for more rigorous comparison, we should take the momentum-dependent top EDM and WDM into account.

Soni and Xu [21] have estimated the top EDM factor $\text{Re}(c)$ in Higgs-boson-exchange models of CP nonconservation to be typically of the order of 10^{-3} – 10^{-4} , which is still much smaller than the experimental sensitivities in the processes $e^+e^- \rightarrow \gamma^* \rightarrow t\bar{t}$ for the total integrated luminosity 20 fb^{-1} and the cm. energy $\sqrt{s} = 500 \text{ GeV}$. However, as indicated in Table 3 and Figure 10, the two-photon mode is expected to greatly improve the experimental constraints on the T-odd top-quark EDM by increasing the cm. energy and by adjusting the laser beam frequency.

Acknowledgments

The authors would like to thank F. Cuyppers, M. Drees, K. Hagiwara, S. D. Rindani, H. S. Song, and P. Zerwas for helpful discussions. The work was supported in part by the KOSEF-DFG large collaboration project (Project No. 96-0702-01-01-2) and Center for Theoretical Physics (CTP). MSB is a postdoctoral fellow supported by KOSEF and Research University Fund of College of Science at Yonsei University supported by MOE of Korea. The work of SYC was supported in part by KOSEF and Korean Federation of Science and Technology Societies through the Brain Pool program and the work of CSK was supported in part by BSRIP program (Project No. BSR I-97-2425).

A The definition and explicit analytic form of P_X

The definition of P_X ($X = 1$ to 16 and $X = L; R$) in terms of the helicity amplitudes M^X ($X = L; R$ and $\gamma = h, i$) is as follows

$$\begin{aligned}
P_{1X} &= \frac{1}{4} M_{++}^{Xh} f + M_{++}^{Xi} f + M_{+}^{Xh} f + M_{+}^{Xi} f^i; \\
P_{2X} &= \frac{1}{3} \text{Re}(M_{++}^{Xh} M_{++}^{Xh}) + \frac{1}{4} (M_{++}^{Xh} f + M_{++}^{Xi} f - M_{+}^{Xh} f - M_{+}^{Xi} f); \\
P_{3X} &= \frac{1}{2} \text{Re}(M_{++}^{Xh} + M_{+}^{Xh})(M_{+}^{Xi} + M_{+}^{Xi}); \\
P_{4X} &= \frac{1}{2} \text{Re}(M_{++}^{Xh} - M_{+}^{Xh})(M_{+}^{Xi} - M_{+}^{Xi}); \\
P_{5X} &= \frac{1}{2} \text{Im}(M_{++}^{Xh} + M_{+}^{Xh})(M_{+}^{Xi} - M_{+}^{Xi}); \\
P_{6X} &= \frac{1}{2} \text{Im}(M_{++}^{Xh} - M_{+}^{Xh})(M_{+}^{Xi} + M_{+}^{Xi}); \\
P_{7X} &= \frac{1}{2} M_{++}^{Xh} f - M_{+}^{Xh} f^i; \\
P_{8X} &= \frac{1}{2} M_{+}^{Xh} f - M_{++}^{Xi} f^i; \\
P_{9X} &= \frac{1}{3} \text{Re}(M_{++}^{Xh} M_{++}^{Xh}) - \frac{1}{2} (M_{++}^{Xh} f + M_{++}^{Xi} f - M_{+}^{Xh} f - M_{+}^{Xi} f);
\end{aligned}$$

$$\begin{aligned}
P_{10X} &= \frac{1}{3} \frac{P}{2} \text{Re } M_{++}^X M_{++}^X ; \\
P_{11X} &= \frac{1}{3} \frac{P}{2} \text{Im } M_{++}^X M_{++}^X ; \\
P_{12X} &= \frac{1}{3} \frac{P}{2} \text{Im } M_{++}^X M_{++}^X ; \\
P_{13X} &= \frac{1}{6} \frac{P}{2} \text{Im } (M_{++}^X M_{++}^X) (M_{++}^X M_{++}^X)^i ; \\
P_{14X} &= \frac{1}{6} \frac{P}{2} \text{Im } (M_{++}^X + M_{++}^X) (M_{++}^X + M_{++}^X)^i ; \\
P_{15X} &= \frac{1}{6} \frac{P}{2} \text{Re } (M_{++}^X M_{++}^X) (M_{++}^X + M_{++}^X)^i ; \\
P_{16X} &= \frac{1}{6} \frac{P}{2} \text{Re } (M_{++}^X + M_{++}^X) (M_{++}^X M_{++}^X)^i ;
\end{aligned} \tag{123}$$

It is simple to derive all the P_X term up to linear in c and c_z from the helicity amplitudes of $e^+e^- \rightarrow \mu\mu$, neglecting higher-order terms in the form factors. In the linear approximation, the CP-even and CP-odd terms independent of c and c_z are given by

$$\begin{aligned}
P_{1L,R} &= \frac{1}{2} (v_{L,R}^2 + 2a_{L,R}^2) (1 + \cos^2 \theta) - 2 v_{L,R} a_{L,R} \cos \theta \\
&\quad + \frac{1}{2} (1 - \cos^2 \theta) v_{L,R}^2 \sin^2 \theta ; \\
P_{2L,R} &= \frac{1}{3} \frac{P}{3} \frac{1}{2} (v_{L,R}^2 + 2a_{L,R}^2) (1 + \cos^2 \theta) - 2 v_{L,R} a_{L,R} \cos \theta \\
&\quad + \frac{1}{2} (1 - \cos^2 \theta) v_{L,R}^2 \sin^2 \theta ; \\
P_{4L,R} &= \frac{2}{6} v_{L,R} (a_{L,R} \cos \theta - v_{L,R}) \sin \theta ; \\
P_{8L,R} &= \frac{2}{6} v_{L,R} a_{L,R} (1 + \cos^2 \theta) - (v_{L,R}^2 + 2a_{L,R}^2) \cos \theta^i ; \\
P_{9L,R} &= \frac{1}{3} \frac{P}{6} (v_{L,R}^2 + 2a_{L,R}^2) (1 + \cos^2 \theta) - 4 v_{L,R} a_{L,R} \cos \theta \\
&\quad - 2 (1 - \cos^2 \theta) v_{L,R}^2 \sin^2 \theta^i ; \\
P_{10L,R} &= \frac{1}{3} \frac{P}{2} (v_{L,R}^2 - 2a_{L,R}^2) \sin^2 \theta ; \\
P_{15L,R} &= \frac{P}{3} \frac{2}{2} v_{L,R} (v_{L,R} \cos \theta - a_{L,R}) \sin \theta ;
\end{aligned} \tag{124}$$

where $v_{L,R}$, $a_{L,R}$ and $c_{L,R}$ are defined in Eqs. (15) and (16).

Every CP-even and CP-odd term vanishes at the tree level:

$$P_{6L} = P_{6R} = P_{11L} = P_{11R} = P_{13L} = P_{13R} = 0; \tag{125}$$

These T -odd terms can have finite contributions from QCD or QED loop corrections[7] through the absorptive parts in the amplitude so that the terms can provide an important QCD test since the dominant contributions are from one-loop QCD contributions.

Every CP-odd and CPT-even term P_X , which depends on the real parts of c and c_z is given by

$$\begin{aligned} P_{5L,R} &= \frac{\sqrt{6}}{3} (a_{L,R} \cos \theta_{L,R} - v_{L,R}) \sin \theta_{L,R} \operatorname{Re}(c_{L,R}); \\ P_{12L,R} &= \frac{\sqrt{2}}{6} v_{L,R} \sin^2 \theta_{L,R} \operatorname{Re}(c_{L,R}); \\ P_{14L,R} &= \frac{\sqrt{2}}{3} (v_{L,R} \cos \theta_{L,R} - a_{L,R}) \sin \theta_{L,R} \operatorname{Re}(c_{L,R}); \end{aligned} \quad (126)$$

whereas every CP-odd and CPT-odd term P_X , which depends on the imaginary parts of the form factors, c and c_z , is given by

$$\begin{aligned} P_{3L,R} &= \frac{\sqrt{6}}{3} (v_{L,R} \cos \theta_{L,R} - a_{L,R}) \sin \theta_{L,R} \operatorname{Im}(c_{L,R}); \\ P_{7L,R} &= \frac{\sqrt{2}}{3} v_{L,R} \sin^2 \theta_{L,R} \operatorname{Im}(c_{L,R}); \\ P_{16L,R} &= \frac{\sqrt{2}}{3} (a_{L,R} \cos \theta_{L,R} - v_{L,R}) \sin \theta_{L,R} \operatorname{Im}(c_{L,R}); \end{aligned} \quad (127)$$

B The definition of angular correlations D_i and D_i^0

For notational convenience we use the following abbreviations

$$\begin{aligned} c_1 &= \sin \theta \cos \phi; & c_2 &= \sin \theta \sin \phi; & c_3 &= \cos \theta; \\ c_1^0 &= \sin \theta \cos \phi; & c_2^0 &= \sin \theta \sin \phi; & c_3^0 &= \cos \theta; \end{aligned} \quad (128)$$

Then the orthonormal decay angular correlations D_i ($i = 1$ to 16) and D_i^0 ($i = 1$ to 12) are defined in terms of c_i and c_i^0 ($i = 1, 2, 3$) as

$$\begin{aligned} D_1 &= 1; & D_2 &= \frac{\sqrt{3}}{2} (c_1^0 c_1 + c_2^0 c_2 + c_3^0 c_3); \\ D_3 &= \frac{\sqrt{3}}{2} (c_1^0 c_1 - c_2^0 c_2); & D_4 &= \frac{\sqrt{3}}{2} (c_1^0 c_1 - c_3^0 c_3); \\ D_5 &= \frac{\sqrt{3}}{2} (c_2^0 c_2 - c_3^0 c_3); & D_6 &= \frac{\sqrt{3}}{2} (c_2^0 c_2 + c_3^0 c_3); \\ D_7 &= \frac{\sqrt{3}}{2} (c_3^0 c_3 - c_1^0 c_1); & D_8 &= \frac{\sqrt{3}}{2} (c_3^0 c_3 - c_2^0 c_2); \\ D_9 &= \frac{\sqrt{3}}{6} (c_1^0 c_1 + c_2^0 c_2 - 2 c_3^0 c_3); & D_{10} &= \frac{\sqrt{3}}{2} (c_1^0 c_1 - c_2^0 c_2); \\ D_{11} &= \frac{\sqrt{3}}{2} (c_1^0 c_1 + c_2^0 c_2); & D_{12} &= \frac{\sqrt{3}}{2} (c_1^0 c_1 - c_2^0 c_2); \end{aligned}$$

$$\begin{aligned}
D_{13} &= \frac{3}{2} (2 \ 3 + 3 \ 2); & D_{14} &= \frac{3}{2} (2 \ 3 \ 3 \ 2); \\
D_{15} &= \frac{3}{2} (3 \ 1 + 1 \ 3); & D_{16} &= \frac{3}{2} (3 \ 1 \ 1 \ 3);
\end{aligned} \tag{129}$$

and

$$\begin{aligned}
D_1^0 &= \frac{3}{2} \frac{\sqrt{5}}{2} (2 \ 3 + 3 \ 2); & D_2^0 &= \frac{15}{2} \frac{\sqrt{5}}{2} (1 \ 2 \ 2 \ 1 + 2 \ 2); \\
D_3^0 &= \frac{15}{2} \frac{\sqrt{5}}{2} (1 \ 2 \ 1 \ 2); & D_4^0 &= \frac{15}{2} \frac{\sqrt{5}}{2} (2 \ 3 \ 2 \ 3); \\
D_5^0 &= \frac{3}{2} \frac{\sqrt{5}}{2} (3 \ 1 \ 3 \ 1); & D_6^0 &= \frac{3}{2} \frac{\sqrt{5}}{2} h_2 (1 \ 2 \ 2) + (1 \ 2 \ 2) \frac{i}{2}; \\
D_7^0 &= \frac{3}{2} \frac{\sqrt{5}}{2} 1 \ 1 (2 \ 2); & D_8^0 &= \frac{15}{2} \frac{\sqrt{5}}{2} h_2 (1 \ 3 \ 3) + (1 \ 3 \ 3) \frac{i}{2}; \\
D_9^0 &= \frac{3}{2} \frac{\sqrt{5}}{2} 3 \ 3 (2 \ 2); & D_{10}^0 &= \frac{3}{2} \frac{\sqrt{5}}{2} (1 \ 2 \ 3 + 1 \ 2 \ 3); \\
D_{11}^0 &= \frac{3}{2} \frac{\sqrt{5}}{2} (2 \ 3 \ 1 + 2 \ 3 \ 1); & D_{12}^0 &= \frac{3}{2} \frac{\sqrt{5}}{2} (3 \ 1 \ 2 + 3 \ 1 \ 2);
\end{aligned} \tag{130}$$

The correlation functions D and D^0 are normalized to satisfy the orthonormality conditions;

$$\begin{aligned}
\int d\Omega \int d\Omega' D_{oi} D_{oj} &= \frac{1}{(4\pi)^2} \int d\Omega \int d\Omega' D_{oi} D_{oj} = \delta_{ij}; \\
\int d\Omega \int d\Omega' D_{oi}^0 D_{oj}^0 &= \frac{1}{(4\pi)^2} \int d\Omega \int d\Omega' D_{oi}^0 D_{oj}^0 = \delta_{ij}; \\
\int d\Omega \int d\Omega' D_{oi}^0 D_{oj} &= \frac{1}{(4\pi)^2} \int d\Omega \int d\Omega' D_{oi}^0 D_{oj} = 0;
\end{aligned} \tag{131}$$

where $(i) = 1$ to 16 and $(j) = 1$ to 12.

References

- [1] F. Abe, et al, Phys. Rev. Lett. 74 (1995) 2662; S. Abachi, et al, Phys. Rev. Lett. 74 (1995) 2662; Particle Data Group, Review of Particle Properties, Phys. Rev. D 54 (1996) 1.
- [2] I. Y. Bigi, Y. L. Dokshitzer, V. Khoze, J. Kuhn and P. Zerwas, Phys. Lett. B 181 (1986) 157.
- [3] W. Bernreuther and M. Suzuki, Rev. Mod. Phys. 63 (1991) 313 and references therein.
- [4] Proceedings of the 1st International Workshop on "Physics and Experiments with Linear e^+e^- Colliders" (Saariselka, Finland, September 1991), eds. R. O'Raifeartaigh, P. Eerola, and M. Nordberg (World Scientific, Singapore, 1992); Proceedings of the 2nd International Workshop on "Physics and Experiments with Linear e^+e^- Colliders" (Waikoloa, Hawaii,

- April 1993), eds. F.A. Harris, S.L. Olsen, S. Pakvasa, and X. Tata (World Scientific, Singapore, 1993), Proceedings of the 3rd International Workshop on "Physics and Experiments with Linear e^+e^- Colliders" (Iwate, Japan, September 1995), eds. A. Miyamoto, Y. Fujii, T. Matsui, and S. Iwata, (World Scientific, Singapore, 1996).
- [5] W. Bernreuther and A. Brandenburg, Phys. Lett. B 314 (1993) 104; W. Bernreuther, J.P. Ma, and B.H.J.M. Kellar, Phys. Rev. D 51 (1995) 2475; H. Anlauf, W. Bernreuther, and A. Brandenburg, Phys. Rev. D 52 (1995) 3803 and references therein.
 - [6] W. Bernreuther and O. Nachtmann, Phys. Rev. Lett. 63 (1989) 2787; W. Bernreuther, O. Nachtmann, P. Overmann and T. Schroder, Nucl. Phys. B 388 (1992) 53.
 - [7] G.L. Kane, G.A. Ladinsky, and C.-P. Yuan, Phys. Rev. D 45 (1992) 124.
 - [8] C.R. Schmidt and M.E. Peskin, Phys. Rev. Lett. 69 (1992) 410; D. Atwood, A. Appel, and A. Soni, Phys. Rev. Lett. 69 (1992) 2754.
 - [9] F. Cuyppers and S.D. Rindani, Phys. Lett. B 343 (1995) 333.
 - [10] P. Poulsen and S.D. Rindani, Phys. Lett. B 349 (1995) 379.
 - [11] S.Y. Choi and K. Hagiwara, Phys. Lett. B 359 (1995) 369.
 - [12] E.P. Shabalin, Sov. J. Nucl. Phys. 28 (1978) 75.
 - [13] For the models with extra scalars, see, for example, J.F. Gunion, H.E. Haber, G. Kane, and S. Dawson, Higgs Hunter's Guide, (Addison-Wesley, Redwood City, CA, 1990).
 - [14] K. Hagiwara and D. Zeppenfeld, Nucl. Phys. B 274 (1986) 1.
 - [15] K. Hikasa, Phys. Lett. B 143, 266 (1984); Phys. Rev. D 33, 3203 (1986).
 - [16] M. Jezabek and J.H. Kuhn, Nucl. Phys. B 320 (1989) 20; A. Czamecki, M. Jezabek and J.H. Kuhn, Nucl. Phys. B 351 (1991) 70.
 - [17] S.Y. Choi, K. Hagiwara and M.S. Baek, Phys. Rev. D 54 (1996) 6703.
 - [18] K. Hagiwara, R.D. Peccei, D. Zeppenfeld and K. Hikasa, Nucl. Phys. B 282 (1987) 253.
 - [19] I.F. Ginzburg, G.L. Kotkin, V.G. Serbo, S.L. Pan'filov and V.I. Telnov, Sov. ZhETF Pis'ma 34, 514 (1981) [JETP Lett. 34, 491 (1982)]; Nucl. Instr. and Meth. 205, 47 (1983); I.F. Ginzburg, G.L. Kotkin, S.L. Pan'filov, V.G. Serbo, and V.I. Telnov, ibid 219, 5 (1984); V.I. Telnov, ibid A 294, 72 (1992).
 - [20] The function A has been considered by M. Kramer, J. Kuhn, M.L. Stong, and P.M. Zerwas, Z. Phys. C 64 (1994) 21.
 - [21] A. Soni and R.M. Xu, Phys. Rev. Lett. 69 (1992) 33.

Tables

Table 1: CP and CPT properties of P_X 's and D_X 's ($X = L, R$ and $i = 1$ to 16).

Table 2: CP and CPT properties of the invariant functions and the angular distributions.

Table 3: The optimal sensitivities to the CP-odd top EDM form factor $\text{Re}(c)$ and their corresponding x values for $\sqrt{s} = 0.5$ and 1 TeV.

Figures

Figure 1: Feynman diagram for the Vtt ($V = \gamma, Z$) vertex.

Figure 2: Schematic view of the sequential processes $e^+e^- \rightarrow t\bar{t} \rightarrow (bW^+)(bW^-) \rightarrow (bl^+\nu_l)(bl^-\nu_l)$. The dashed lines are for invisible particle trajectories in a particle detector.

Figure 3: The 1- allowed region of the CP-odd parameters $\text{Re}(c)$ and $\text{Re}(c_z)$ through the CP-odd and CPT-even asymmetries (a) A_1^b and T_{33}^b and (b) A_1^l and T_{33}^l with polarized electron beams, respectively, for the e^+e^- integrated luminosity 10 fb^{-1} and for the cm. energy $\sqrt{s} = 500 \text{ GeV}$. The solid lines with a positive (negative) slope are for A_1^b and A_1^l with right-handed (left-handed) electrons while the long-dashed lines with a positive (negative) slope are for T_{33}^b and T_{33}^l with right-handed (left-handed) electrons.

Figure 4: The 1- allowed region of the CP-odd parameters $\text{Re}(c)$ and $\text{Re}(c_z)$ through the CP-odd and CPT-even asymmetries (a) A_1^b and T_{33}^b and (b) A_1^l and T_{33}^l with unpolarized electron beams, respectively, for the e^+e^- integrated luminosity 20 fb^{-1} and for the cm. energy $\sqrt{s} = 500 \text{ GeV}$. The solid lines are for A_1^b and A_1^l while the long-dashed lines are for T_{33}^b and T_{33}^l .

Figure 5: The 1- allowed region of the CP-odd parameters $\text{Im}(c)$ and $\text{Im}(c_z)$ through the CP-odd and CPT-odd asymmetries (a) A_E^b, A_2^b and Q_{33}^b and (b) A_E^l, A_2^l and Q_{33}^l with polarized electron beams, respectively, for the e^+e^- integrated luminosity 10 fb^{-1} and for the cm. energy $\sqrt{s} = 500 \text{ GeV}$. The solid lines with a positive (negative) slope are for A_E^b and A_2^b with right-handed (left-handed) electrons while the long-dashed lines with a positive (negative) slope are for A_2^b and A_2^l with right-handed (left-handed) electrons. And, the dot-dashed lines with a positive (negative) slope are for Q_{33}^b and Q_{33}^l with right-handed (left-handed) electrons.

Figure 6: The 1- allowed region of the CP-odd parameters $\text{Im}(c)$ and $\text{Im}(c_z)$ through the CP-odd and CPT-odd asymmetries (a) A_E^b, A_2^b and Q_{33}^b and (b) A_E^l, A_2^l and Q_{33}^l with unpolarized

electron beams, respectively, for the e^+e^- integrated luminosity 20 fb^{-1} and for the c.m. energy $\sqrt{s} = 500 \text{ GeV}$. The solid lines are for A_E^b and A_E^1 while the long-dashed lines are for A_2^b and A_2^1 . And, the dashed lines are for Q_{33}^b and Q_{33}^1 .

Figure 7: The coordinate system in the colliding c.m. frame. The scattering angle, θ , and the azimuthal angles, ϕ_1 and ϕ_2 , for the linear polarization directions measured from the scattering plane are described.

Figure 8: (a) the photon energy spectrum and (b) the degree of linear polarization of the Compton backscattered photon beam for $x = 4E_0/m_e^2 = 0.5, 1$ and 4.83 .

Figure 9: (a) the luminosity spectrum and (b) the two linear polarization transfers, A_1 (solid lines) and A_2 (dashed lines), for $x = 4E_0/m_e^2 = 0.5, 1$ and 4.83 .

Figure 10: The x dependence of the $\text{Re}(c)$ upper bound, $\text{Max}(\text{Re}(c))$, at $\sqrt{s} = 0.5$ and 1 TeV , from the asymmetry A_{00} . The solid line is for $\sqrt{s} = 0.5 \text{ TeV}$ and the long-dashed line for $\sqrt{s} = 1 \text{ TeV}$.

Table 1

CP	CPT	P_x	D	Number
even	even	$P_{1X}; P_{2X}; P_{4X}; P_{8X}$ $P_{9X}; P_{10X}; P_{15X}$	$D_1; D_2; D_4; D_8$ $D_9; D_{10}; D_{15}$	7
even	odd	$P_{6X}; P_{11X}; P_{13X}$	$D_6; D_{11}; D_{13}$	3
odd	even	$P_{5X}; P_{12X}; P_{14X}$	$D_5; D_{12}; D_{14}$	3
odd	odd	$P_{3X}; P_{7X}; P_{16X}$	$D_3; D_7; D_{16}$	3

Table 2

CP	CPT	Invariant functions	Angular dependences
even	even	unpol	
		$\langle \quad \rangle_{02}$	$\cos(\quad + \quad) + \cos(\quad)$
		$\langle \quad \rangle_{22}$	$\cos(2 \quad)$
		$\langle \quad \rangle_{00}$	$\cos(2 \quad)$
even	odd	$= \langle \quad \rangle_{02}$	$\sin(\quad + \quad) + \sin(\quad)$
		$= \langle \quad \rangle_{22}$	$\sin(2 \quad)$
odd	even	$= \langle \quad \rangle_{02}$	$\sin(\quad + \quad) - \sin(\quad)$
		$= \langle \quad \rangle_{00}$	$\sin(2 \quad)$
odd	odd	$\langle \quad \rangle_{02}$	$\cos(\quad + \quad) - \cos(\quad)$

Table 3

p_s	0.5	1.0
x	3.43	0.85
Re(c)	0.16	0.02

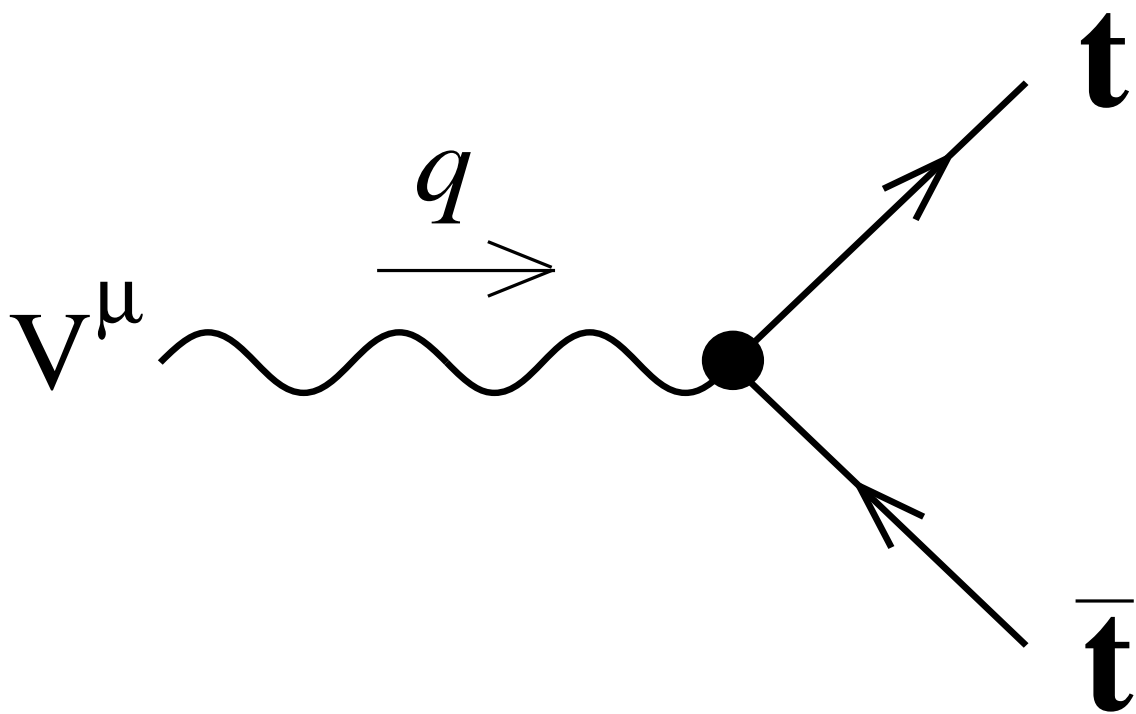


Figure 1

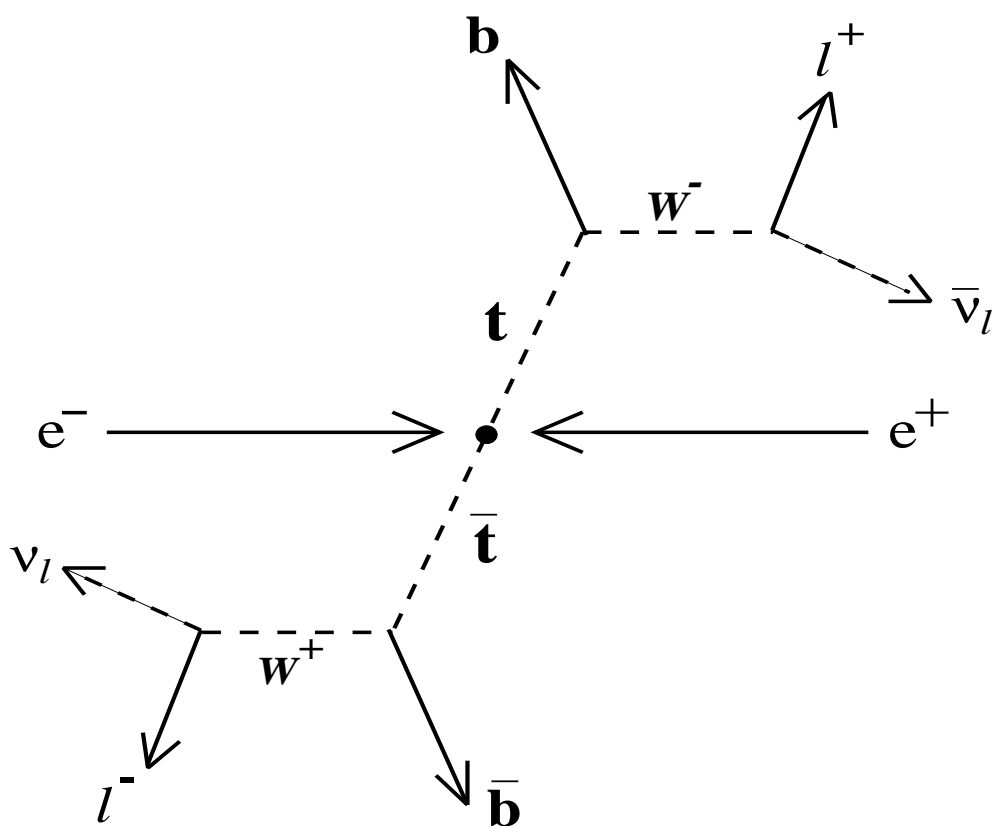


Figure 2

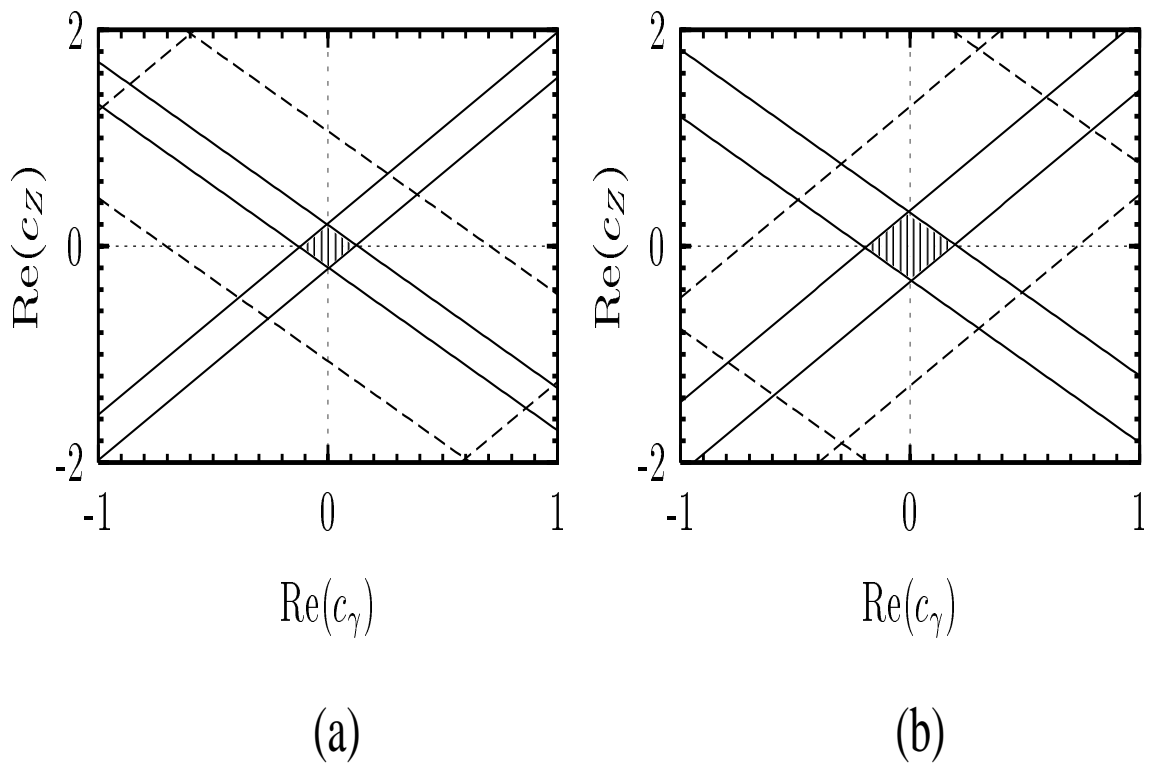


Figure 3

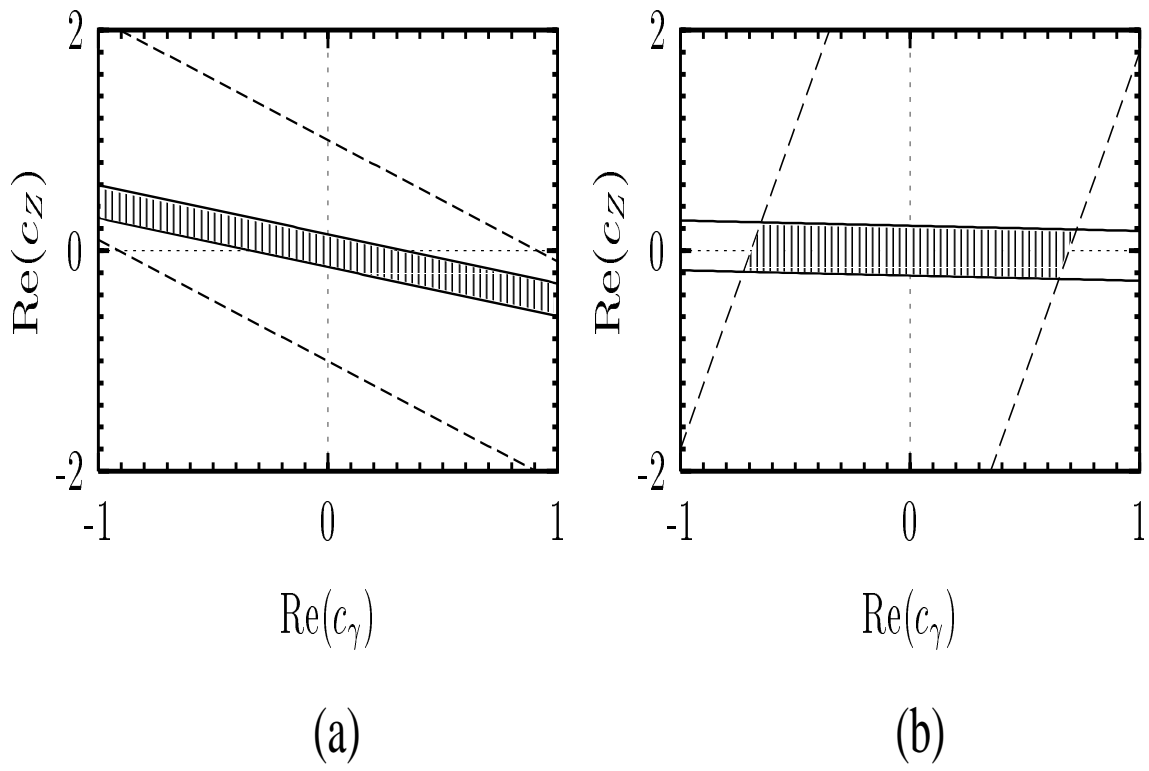


Figure 4

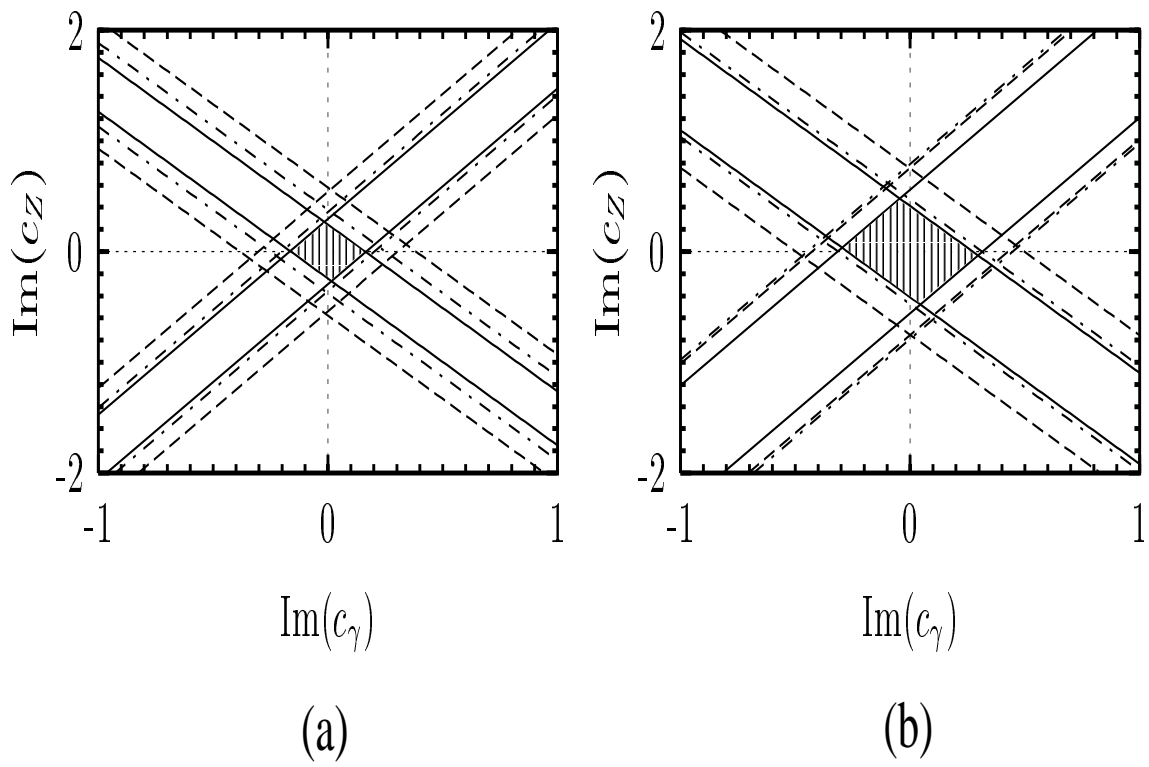


Figure 5

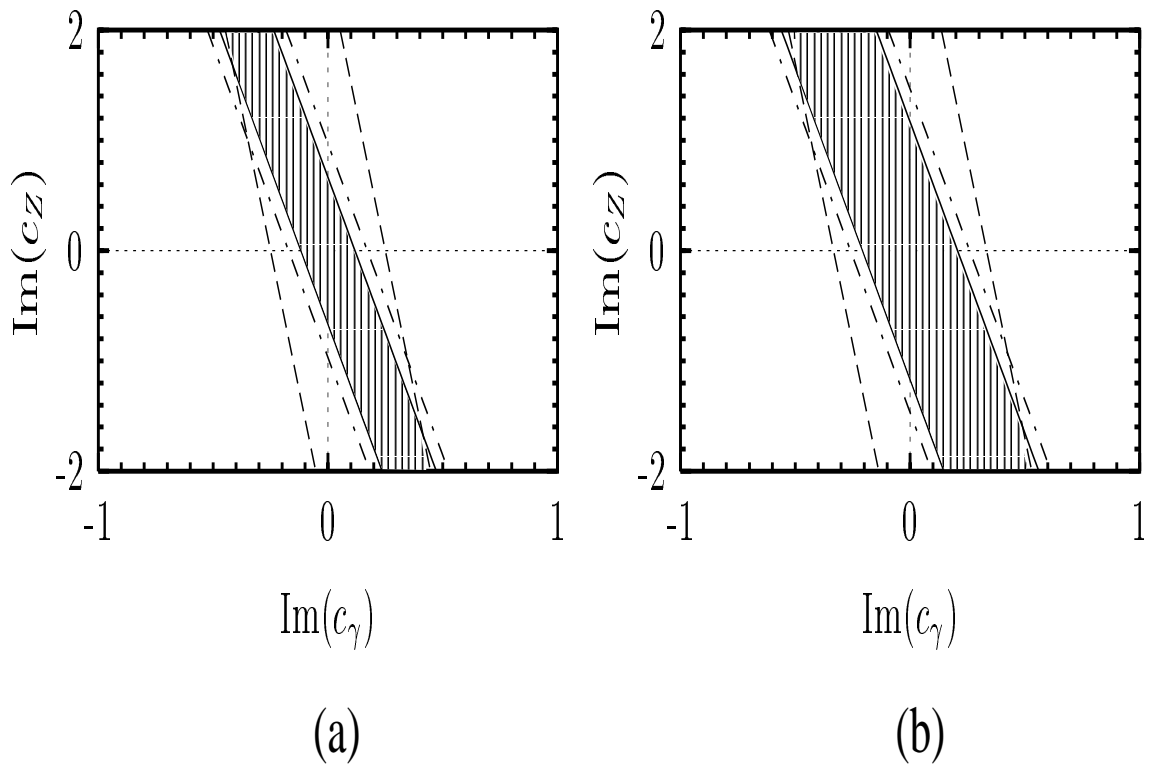


Figure 6

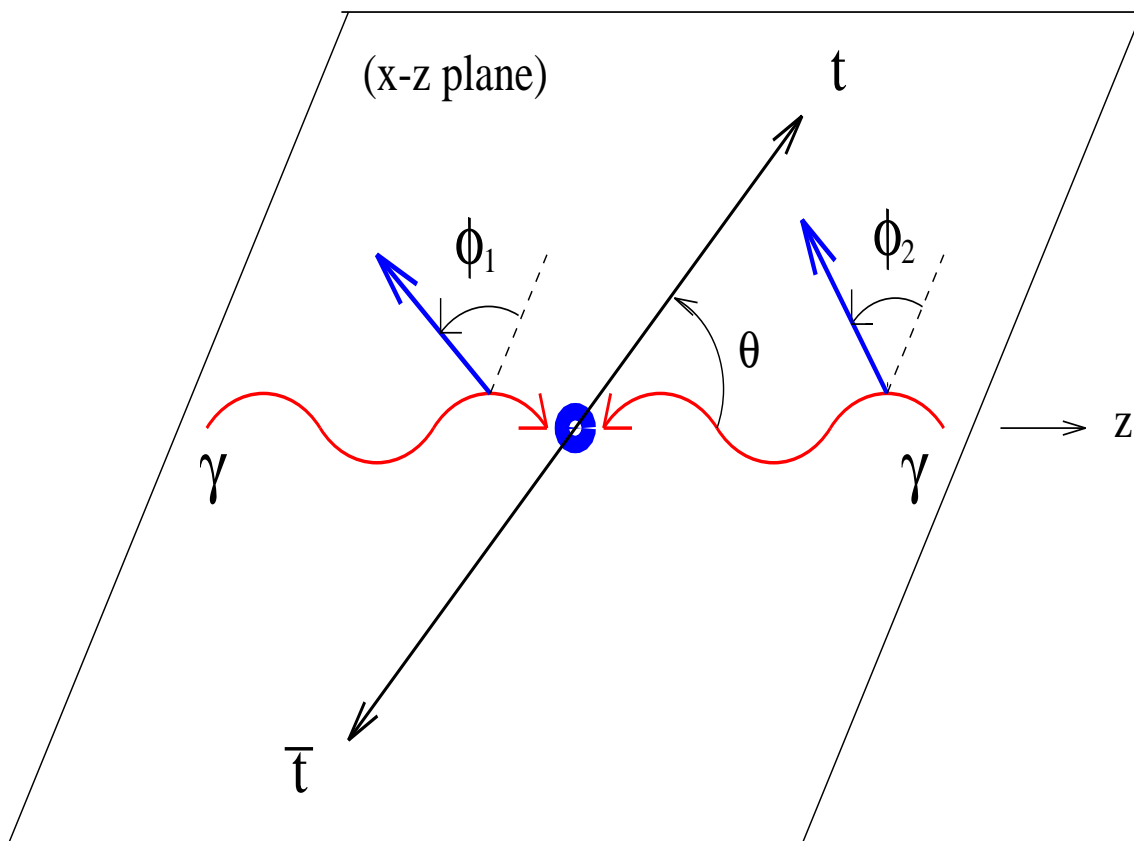


Figure 7

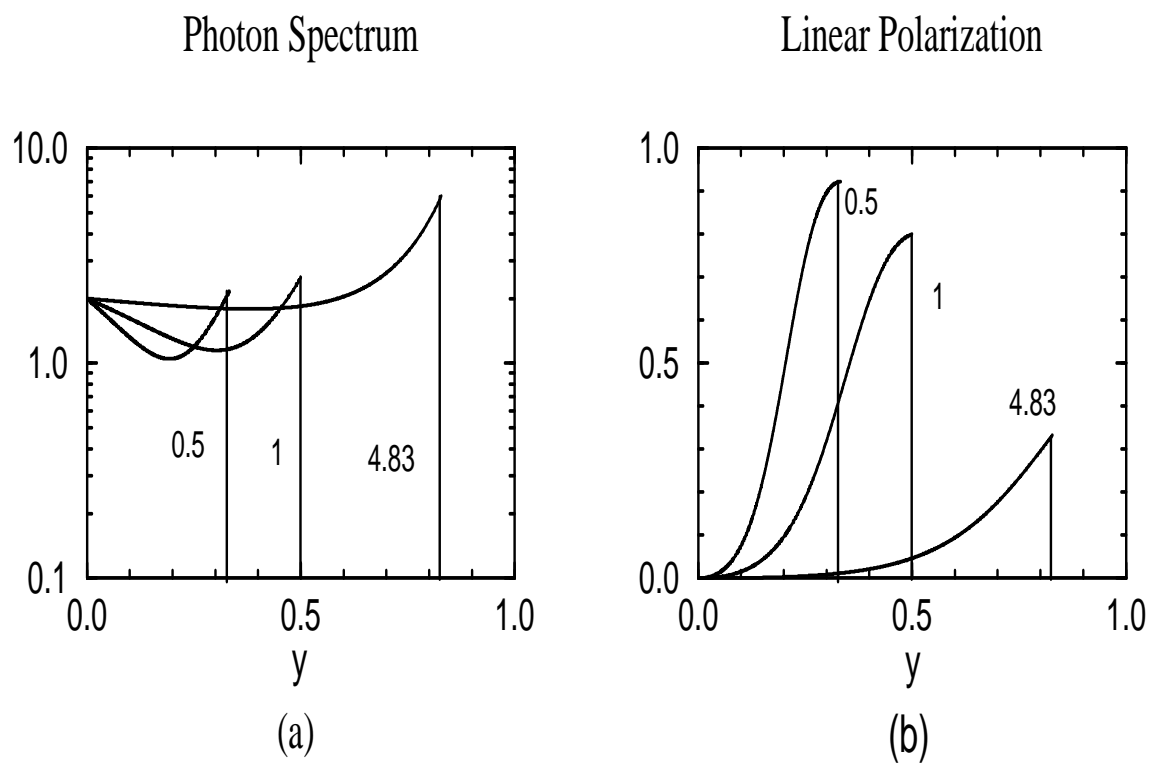


Figure 8

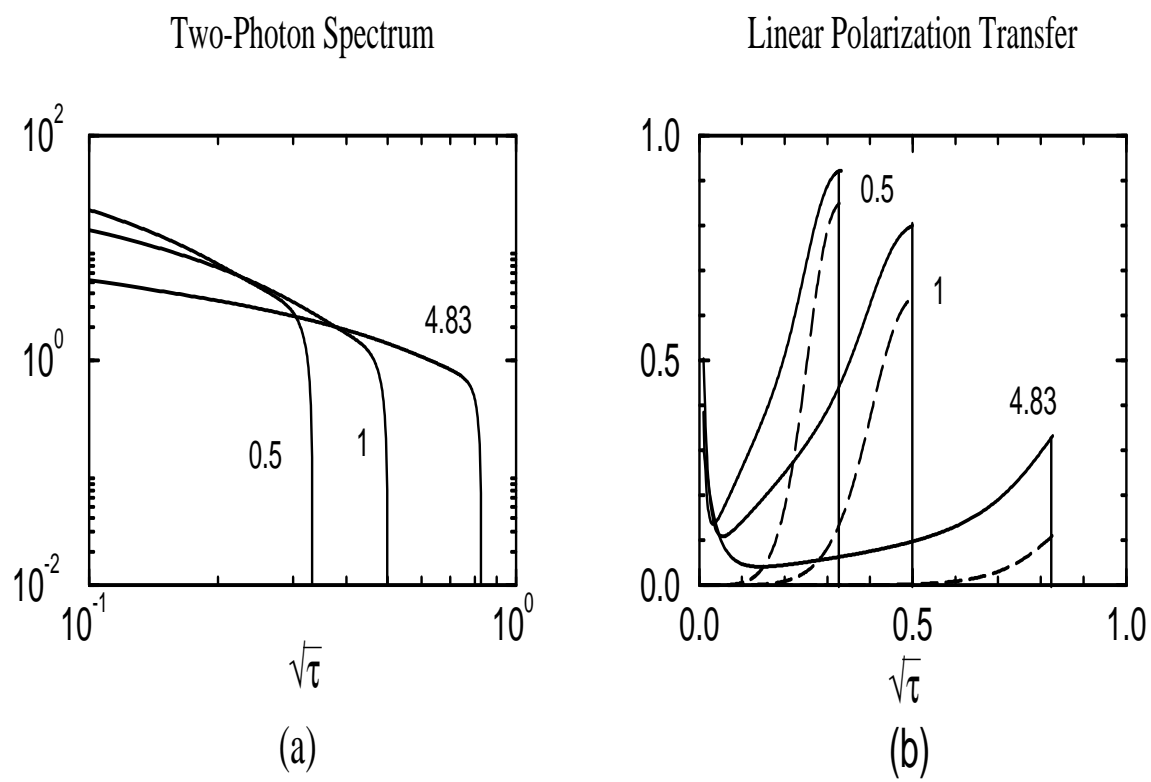


Figure 9

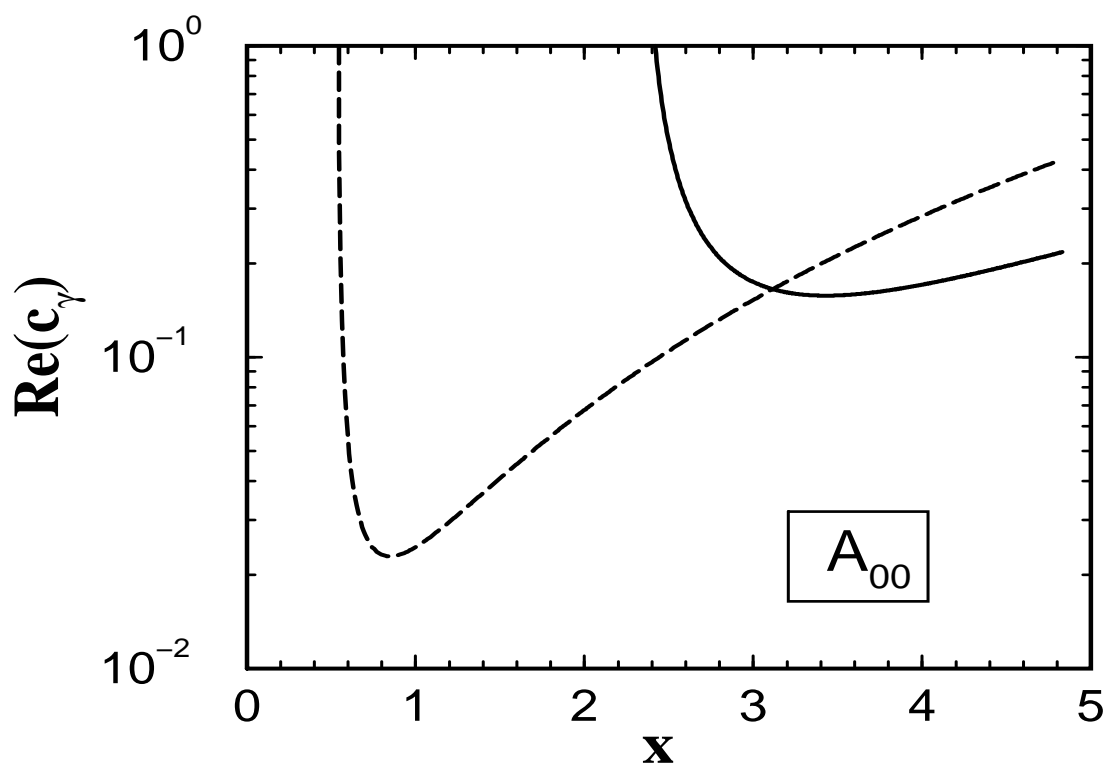


Figure 10